Atmospheric Pollution Research 14 (2023) 101872

Contents lists available at ScienceDirect

Atmospheric Pollution Research

journal homepage: www.elsevier.com/locate/apr

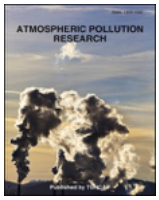

# A novel approach for brake emission estimation based on traffic microsimulation, vehicle system dynamics, and machine learning modeling

Mostafa Rahimi [a,*], Stefano Candeo [a], Mauro Da Lio [a], Francesco Biral [a], Jens Wahlström [b], Daniele Bortoluzzi [a]

[a] Department of Industrial Engineering, University of Trento, 38123, Trento, Italy
[b] Department of Mechanical Engineering, Lund University, 22100, Lund, Sweden

ARTICLE INFO

*Keywords:*
Brake emission
Brake wear
VISSIM
Artificial neural network
Vehicle dynamics
Simulation

ABSTRACT

Brake wear is known as the primary source of traffic-related non-exhaust particle generation. Its generation rate is influenced by parameters at different levels: subsystem (type of brakes, pads, materials, etc.), system (vehicles' dynamics, driving style etc.) and suprasystem (road geometries, traffic parameters, etc.). At the subsystem level, we proposed a neural network brake emission modeling, trained and validated through emission data collected from a reduced-scale dynamometer. At the system level, a model of a car dynamics was developed to calculate the wheels' brake torques and angular velocities. At the suprasystem level, the traffic behavior in a sensitive urban area was characterized experimentally and simulated in a traffic microsimulation software. The vehicle traffic-based records were used to calculate the vehicle dynamic quantities, converted into brake emission through the neural network. To examine the overall traffic impacts on brake emission, the total particle number (PN) and total particle mass were estimated regarding the route choice in the sensitive area and in the whole transportation network. The findings of this study showed significant generation rate of brake emissions (in terms of mass and number) around congested areas (in the order of 10e9 #/s). The brake emission estimation in a real area provides fundamental information to the decision-makers to better insight into the rate of non-exhaust emissions generation.

## 1. Introduction

Particulate matter (PM) is known to be one of the most problematic pollutants worldwide, threatening millions of lives and air quality. The transportation sector, including light/heavy-duty cars, trains, and airplanes, is considered as one of the important sources of particulate matter and has caused significant environmental problems in recent decades (Hula et al., 2021; Moradi, 2021; Timmers and Achten, 2016). The negative impacts of traffic-related PM particles on human health have extensively been emphasized in epidemiological and toxicological studies (De Kok et al., 2005; Gustafsson et al., 2008; Mantecca et al., 2010; Mukherjee and Agrawal, 2017; Sabbir Ahmed et al., 2018). All these health problems are directly linked to the size of these particles and the challenges they can develop for human health. Fine ($PM_{2.5}$, less than 2.5 μm in diameter) and ultrafine (UFP, less than 0.1 μm in diameter) PM particles can easily deposit in the lungs and eventually, penetrate to the human's bloodstream causing untreatable cardiovascular diseases (Sabbir Ahmed et al., 2018). Therefore, an immediate response is needed to reduce the adverse impacts of such emissions on air pollution. Given the importance of this issue, decision-makers have introduced new and restrictive regulations to not only control but also reduce the rate of traffic-related PM particles, especially in high congested cities. In Europe, dissuasive attempts against PM particles have been made for more than a century, where PM emissions were responsible for 406 thousand premature deaths in 2010 (EC, 2013; Wang et al., 2016). In the United States, regarding the Environmental Protection Agency (EPA) regulations, the amount of PM produced by passenger cars must be reduced by 30% from 2017 to 2025 (Kuklinska et al., 2015).

Vehicle-originated PM emissions are classified into two categories depending on the source nature: First, exhaust PM emissions, which are generated in the vehicle engine due to non-ideal fuel combustion. Second, non-exhaust PM emissions, which consist of particles originating

Peer review under responsibility of Turkish National Committee for Air Pollution Research and Control.
* Corresponding author. Department of Industrial Engineering, University of Trento, Via Sommarive, Povo, 9 - 38123, Trento, Italy.
*E-mail address:* mostafa.rahimi@unitn.it (M. Rahimi).

https://doi.org/10.1016/j.apr.2023.101872
Received 14 February 2023; Received in revised form 29 July 2023; Accepted 29 July 2023
Available online 4 August 2023

from the braking system, tires, clutch, and road dust resuspension. Although the negative effects of exhaust PMs were more regarded in the literature, it is crucial not to overlook the detrimental impacts of non-exhaust PMs. Exhaust-origin PM particles contribute as much and mostly less than non-exhaust PMs to the PM concentrations in urban areas (Amato et al., 2014). Ketzel et al. reported that approximately 50–85 percent of total traffic-related $PM_{10}$ particles in European countries stems from non-exhaust sources depending on the region (Ketzel et al., 2005).

Brake emission, mainly generated by the braking system (disc and pads), holds one of the highest contributions in non-exhaust PM particles (Singh et al., 2020). It has been reported that up to 55% of total non-exhaust traffic $PM_{10}$ emissions are due to brake wear (Grigoratos and Giorgio, 2014). The contribution may become more critical in populated cities, where huge numbers of commuters daily use private or public transportation fleets, making the road significantly more congested, in turn, emitting more brake emissions into the air (Kutlimuratov et al., 2021). Restrictive rules are being regulated to reduce the amount of brake wear in developed countries. For instance, the European Union will regulate brake particle emissions from vehicles up to 3.5 t with EURO7 ($PM_{10}$ limit value of 7 mg/km/vehicle starting 2025 down to 3 mg/km/vehicle in 2035) (EC, 2023). However, numerous previous studies have reported various contributions of brake wear to ambient $PM_{10}$ concentrations from negligible up to 4 $\mu g/m^3$ (Grigoratos and Martini, 2015). Conversely, these proportions are higher in traffic congested spots (Ketzel et al., 2005). In the first view, this level of brake wear contribution may be considered as trivial regarding its two-bit mass. However, its massive bioreactivity resulting severe health concerns, especially in congested areas, could be the primary reason for scientists to extensively take brake wear investigations into account.

Generally, the rate of brake wear generation can be investigated at three levels: First, subsystem level, which deals with the behavior of the braking system components in wear production. Second, system level, which is related to the investigation of wear released by a real car, and third, environmental level that mainly focuses on on-road measurements (Rahimi et al., 2021). Regarding the complexity of monitoring the behavior of wear particles at the system level, the majority of investigations in the literature have been carried out at the subsystem level. Using a simulation-based model like Finite Element Analysis (FEA) is one of the well-known approaches to simulating the brake wear behavior at the subsystem level (Han et al., 2017; Riva et al., 2019; Wahlström et al., 2009). Also, implementing tribological tests on dynamometer machines, a well-known machine for simulating vehicle braking systems in the laboratory environment, has remarkably been regarded in previous studies (Agudelo et al., 2018; Mathissen et al., 2019; Rahimi et al., 2021; Sanders et al., 2002). Regarding the widespread use of dynamometers braking system simulators, a global technical regulation for measuring brake wear particle emissions on a brake dynamometer was published recently (10/2022) to allow comparing brake emissions in a standardized way (UNECE, 2022).

Although previous models showed reasonably reliable results, the broad influential impacts of the real vehicle characteristics on the rate of emitted particles while driving in a real transportation network have been neglected. An alternative for simulation of real driving behaviors can be the implementation of driving simulators. However, they not only impose high costs but also are not capable of integrating with the other platforms like subsystem tribological tests at different levels. Traffic microsimulation models have been introduced as a reliable and efficient tool playing a crucial role in simulating every traffic-related element at the system level (i.e. the vehicle) and suprasystem level (i.e. the traffic) (Alvanchi et al., 2019; Karabag et al., 2020; Kutlimuratov et al., 2021).

Numerous studies in the literature have used traffic microsimulation models to estimate exhaust emissions. Nevertheless, none of them has tried investigating the possibility of non-exhaust emission estimation using traffic simulation-based models. In contrast to exhaust emissions, non-exhaust emission estimation cannot be done without considering the effects of vehicle dynamics on the rate of brake wear generation. These impacts are not negligible because vehicle design features like mass, length, height, and distance of front and rear axles can significantly influence brake wear release rate during vehicle activities. Kinematic parameters like speed and deceleration are also included in this issue. Electric and hybrid vehicles, which recharge batteries during deceleration, reduce the use of brakes (which remain only for emergency brakes) and, hence, can significantly reduce wear particles emissions (Bondorf et al., 2023). Once the vehicle behavior in the traffic environment is determined by means of the microsimulation, considering the vehicle dynamics at the system level makes the estimations much closer to reality.

To make the brake wear estimations more accurate, an alternative can be the integration of different investigation levels. Nevertheless, due to the complexity of such models and the inaccessibility of necessary tools, no significant effort has been put into developing these models in emission estimation so far. As a result, the generalizability of previous studies' conclusions is questionable when limiting their investigations to a particular level. Second, the drawbacks of dependence on lab tests to simulate real driving conditions are previously shown as they are mostly crippled in considering substantial elements (Moradi and Miranda-Moreno, 2020). These elements may include road geometry, traffic conditions, and driving styles. Third, analyzing and understanding the non-linear dependencies corresponding to brake wear generation needs complex AI (Artificial Intelligence)-based models, which traditional statistical modeling techniques cannot answer.

In response to previous studies' limitations and to obtain more reliable brake wear estimation results, this study aims to predict the braking system emissions by implementing a downstream approach (Rahimi, 2023). This novel approach starts from the suprasystem level (microscopic traffic simulation models) and then, focuses on the system level (vehicle dynamics) where the subsystem level (braking system) is modeled. The brake emission is modeled with a neural network properly trained and validated on emission data collected by the experimental tribological tests on reduced-scale dynamometer machine (hereafter "minidyno"). In the following sections, first, the proposed method will be discussed in detail. Then, the tribological tests in the subsystem level and related artificial neural network (ANN) model will be presented. Next, we will penetrate the suprasystem level by proposing ground-truth measurements in a case study and introduce the related traffic microsimulation. The vehicle dynamics model is used as an interface between the aforementioned levels, to convert the single vehicle in-traffic behavior into the relevant functional quantities of the braking system. The last part of the paper will present the brake emission estimation results of all agents with different route decisions in the case study. Lastly, all the findings will be discussed and concluded.

## 2. Proposed method

The method proposed in this research consists of combining three phases of brake wear investigation: suprasystem, system and subsystem levels. At the subsystem level, first, more than one thousand tribological tests are conducted using the minidyno machine. These tests are carried out considering speed, torque, pressure, and other functional parameters to measure the amount of airborne brake wear particles generated for every brake operation and serve for training a neural network emission model. Second, the most useful variables (initial speeds, final speeds, and brake torques) are selected as independent variables to predict the brake emissions using the approximant artificial neural network model. At the suprasystem level, first, real traffic data were collected in a high-congested area in Trento (Italy) in peak hours to identify field specifications. For instance, traffic-related data such as input volume, route choices, pedestrian volumes, modal splits, number of parking lots, traffic light green and red timings are identified. Non-traffic data are also acquired, such as road geometry, field scope, land use, and weather

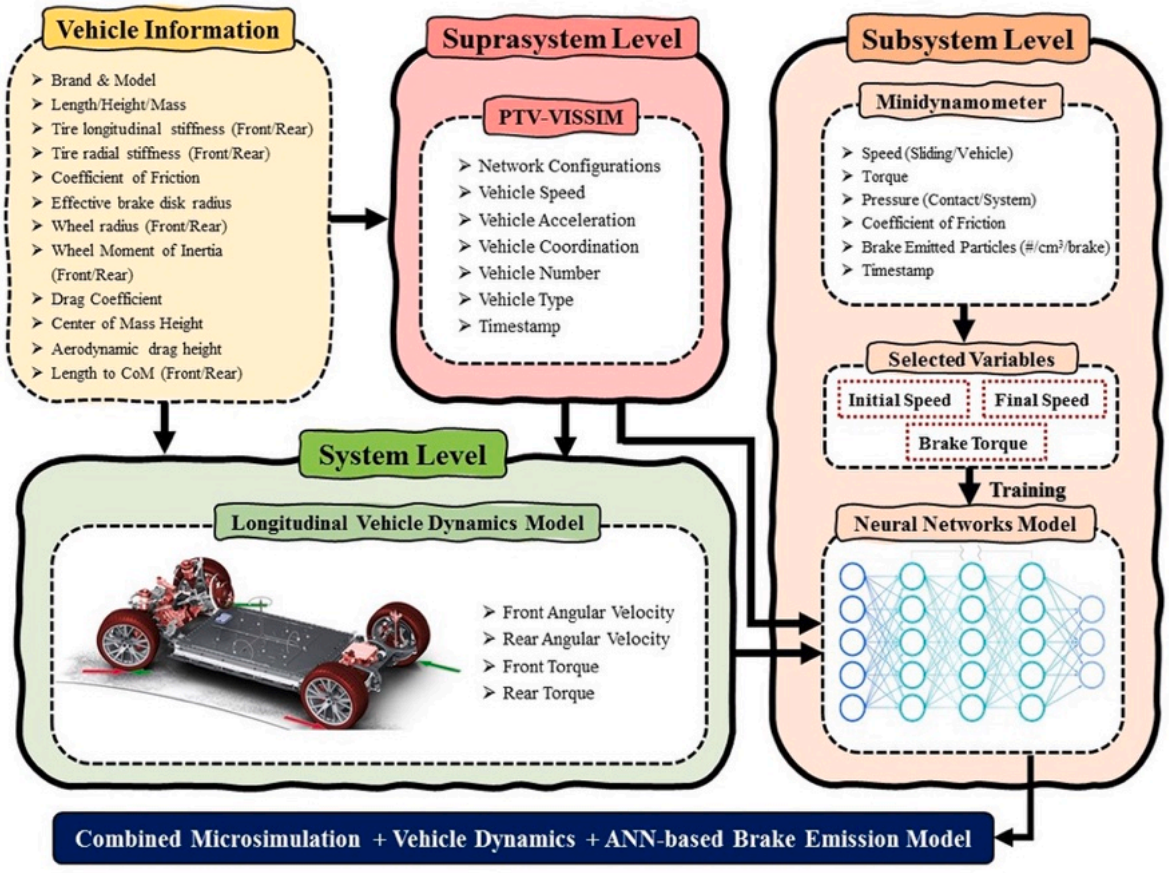


**Fig. 1.** Different steps of the proposed method.

**Table 1**
Targeted vehicle information.

| Parameter | Value | Parameter | Value |
|---|---|---|---|
| Drag coefficient | 0.36 | Vehicle Mass | 2060 *Kg* |
| Nominal radius of the front wheel | 0.37 *m* | Height of the center of mass | 0.712 *m* |
| Radial stiffness of the front tire | 218000 *N/m* | Height of the direction of application of the aerodynamic drag | 1.2 *m* |
| Nominal radius of the rear wheel | 0.37 *m* | Distance between front axle and center of mass | 1.5219 *m* |
| Radial stiffness of the rear tire | 218000 *N/m* | Distance between rear axle and center of mass | 1.3381 *m* |
| Front tire longitudinal stiffness | 30.6217 *N/slip unit* | Front wheel moment of inertia | 1.65 $Kg.m^2$ |
| Rear tire longitudinal stiffness | 30.6217 *N/slip unit* | Rear wheel moment of inertia | 1.65 $Kg.m^2$ |
| Front tire coefficient of rolling resistance | 0.0124 | Braking torque front/ rear axles distribution | 52% |
| Rear tire coefficient of rolling resistance | 0.0124 | Friction coefficient between brake pads | 0.35 |
| Average fuel mass | 70 kg | Average payload mass | 366 kg |

conditions. In the next step, all the obtained data are inserted into the traffic microsimulation software for monitoring the vehicles' trajectories and finding the route choice decisions. To ensure the accuracy of data collection, every single traffic element is modeled in the traffic microsimulation software, and the movements of the network's agents are recorded every 0.05 s. Vehicle records of a dominant sport utility vehicle (SUV) family cars, including vehicle coordination, speed, acceleration, number, length, height, mass, width, and positions in the networks, are accurately extracted from the microsimulation model.

A custom vehicle longitudinal dynamics model is developed, in order to provide its inverse dynamic, i.e. convert its kinematic behavior into the brake activation quantities. Real vehicle information, such as wheels radius, drag coefficient, center of mass height, wheel moment of inertia, coefficient of friction and other related information released by the vehicle manufacturer and published material are collected. The vehicle inverse dynamics model calculates the vehicle's front/rear wheels' brake torques and angular velocities starting from the vehicle speed time-series previously obtained by the traffic microsimulation model. Next, selected vehicle data (brake torques, initial and final speeds for every brake event) obtained by the combination of the microsimulation and vehicle inverse dynamics models are fed to the subsystem level ANN (Artificial Neural Network)-based model to estimate the brake emission in every event. In the final step, the obtained results are comprehensively analyzed in the frame of the traffic environment and concluded. The findings of this research open an innovative and efficacious way for traffic engineers and environmental scientists to study the real brake emissions besides exhaust emissions in various traffic conditions. This study can also be beneficial for the decision-makers to predict and control the amount of brake emission released by either motor vehicles or electric cars day-to-day in order to reduce air pollution and improve the air quality in urban areas. Fig. 1 summarizes the steps of the proposed method.

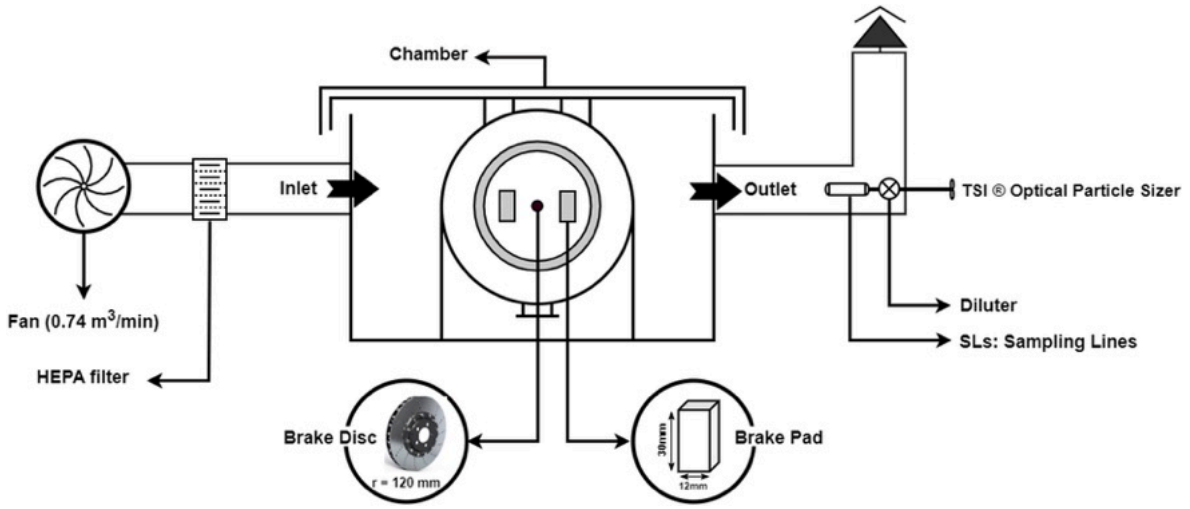


**Fig. 2.** Scheme of the minidyno experimental setup.

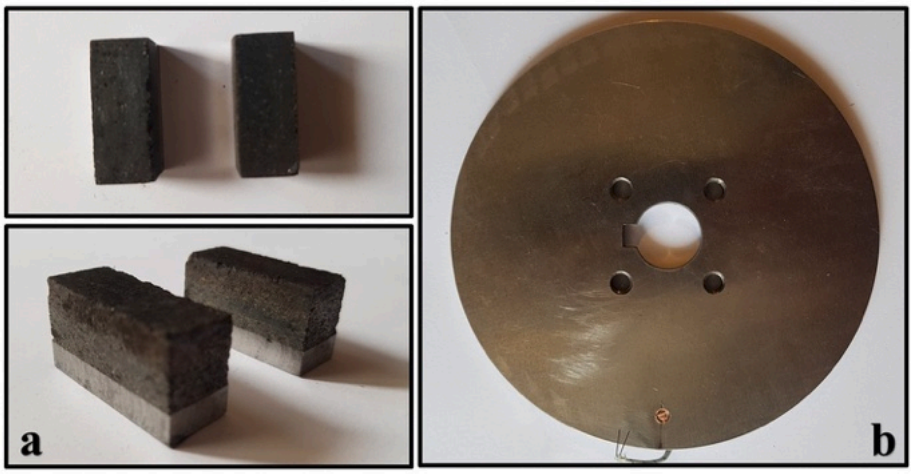


**Fig. 3.** Minidyno main components; a: Brake pads, b: Brake disc.

## 3. Materials and models specifications

In this research, the main contribution consists of a combination of models and materials at suprasystem, system and subsystem levels. The research team used reduced-scale dynamometer to measure the vehicle brake emitted particles at the subsystem level in a set of conditions reproducing typical brake use. Also, PTV-VISSIM traffic microsimulation software and the longitudinal vehicle dynamics model were implemented at the suprasystem and system level, respectively.

### 3.1. Targeted vehicle

Vehicle design characteristics can show remarkable impacts on the generation rate of air pollutant emissions. To approach reality, this information is essential to use as necessary inputs in microsimulation software and longitudinal vehicle dynamics model. In the present study, the authors targeted and investigated a very common SUV family car to estimate brake emission. Table 1 includes all the targeted vehicle information used in this study.

### 3.2. Subsystem level

#### 3.2.1. Minidyno

Besides all merits of using full-scale dynamometers, reduced-scale dynamometers, also known as small-scale dynamometers and minidynos, were widely regarded in previous studies (Rahimi et al., 2021). In 2001, Sanders et al. investigated the frictional characteristics of lining materials using a reduced-scale dynamometer (Sanders et al., 2001). Candeo et al. investigated contact friction and airborne brake wear during a bedding stage for Cu-free brake pads using the LINK minidyno machine model 1200 (Candeo et al., 2021a,b). The same dynamometer machine was also used to build brake performance maps in various scorching conditions of brake pads (Candeo et al., 2021a,b; Varriale et al., 2022). According to previous studies, minidynos can present acceptable and reliable results for the investigation of the braking system (Alnaqi et al., 2015).

In the present study, the research team used the LINK minidyno model 1200 for the tribological tests. This minidyno consists of confining chamber containing a piston and a reduced-scale brake system (two rectangular pads and a disc). The machine can work with plenty of hardware and devices that must be installed to shape an integrated system. Fig. 2 shows the scheme of the system with all its components.

As shown in Fig. 2, a fan providing an airflow rate of 0.74 $m^3$/min was used on the left side of system. A high-efficiency particulate air filter called HEPA subsequently filtered the generated airflow. A sealed chamber confined the braking system providing an ambiance to convey almost all the generated particles to a designated outlet. Inside the outlet large-diameter pipe, sampling probes, and a diluter were installed to

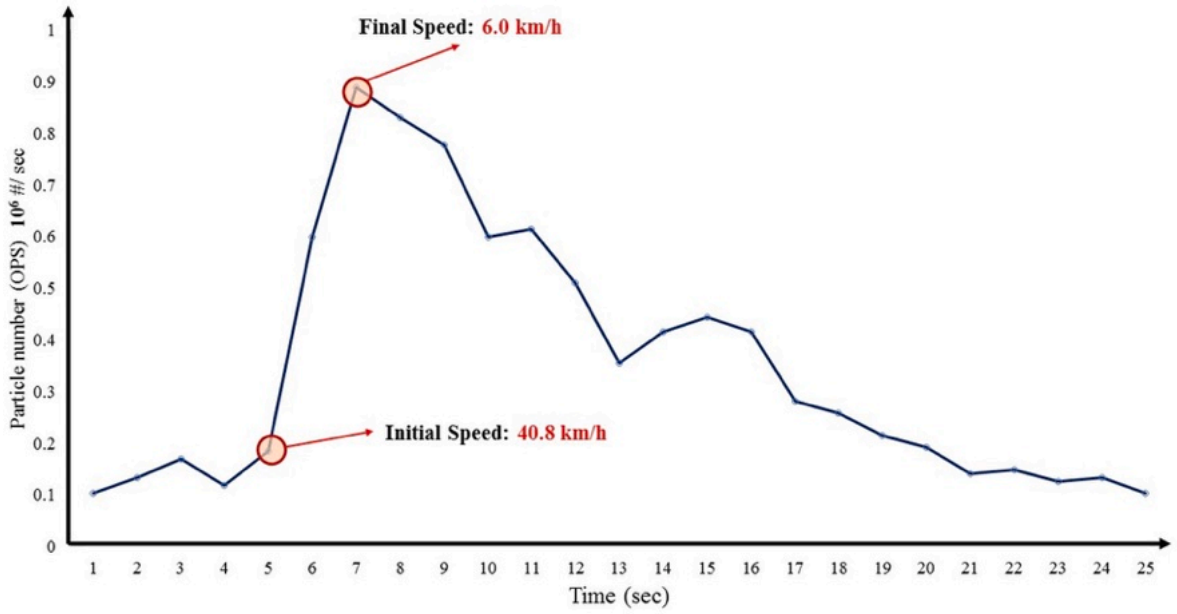


**Fig. 4.** An example of the emission generation in a brake event collected by OPS device in minidyno tests.

help the TSI Optical Particle Sizer (OPS) collect the emissions' data. OPS device can only count particle sizes from 0.3 to 10 μm (in 16 size channels). This captures most of the particles that contributes to the $PM_{10}$ and $PM_{2.5}$, but no nano-sized particles can be registered. The particles with sizes below 0.3 μm contributes most to the numbers of particles generated, at least at higher temperatures.

The brake pads, which were one of the most common commercial low-metallic pads in the market, were cut into rectangular-shaped samples with a geometry size of 12 mm × 30 mm. A conventional pearlitic cast-iron brake disc with the diameter, thickness, effective radius, and hardness of 120 mm, 6 mm, 50 mm, and 235 HV10, respectively, was also used to simulate the movements of the vehicle's brake rotor. Fig. 3 shows the brake pads and disc used for the experiments implemented by minidyno.

To build an ANN brake emission model, the research team defined and configured more than one thousand scenarios for minidyno tests, which boosted the accuracy of the data training. The tribological tests were designed based on the randomization of initial vehicles' speed (60-30 km/h), speed variation (velocity drops) (40-10 km/h), and deceleration (0.9–3.9 m/s$^2$). Also, a threshold temperature (100 °C) was set for the machine as the starting time of the braking events (details can be found in Section 4.1). Tribological parameters such as rotor speed, contact temperature, contact pressure, and deceleration were among the recorded parameters. Fig. 4 demonstrates the number of emissions generated in a brake event per second as measured by OPS device.

### 3.2.2. Data preparation

In addition to the emission generation during brake duration, it was found that the emission would continue to be released even after brake operation. This critical phenomenon may be produced by several factors, like intrinsic dynamics of the particle release mechanism, possible presence of dead air regions with following increase of residence time, etc. To address this issue, by using OPS device, all brake wear was collected for considerably longer periods compared to the brake duration but not exceeding the cycle length of the brake operation.

In minidyno dataset, all tests with a cycle length more than 20 s were removed from the data set (20 tests out of 1000 tests were dropped) in order to prepare the data needed for the synchronization. Data visualization showed that the majority of brakes were operated in less than 8 s. After plotting the whole cycle length of different braking events, it was found that an emission background noise is present, which could be identified analyzing the measured signal before and after the braking period. This makes the identification of braking events complicated and challenging for emission collection. The persistence of emission signal after the brake event and the presence of the emission background noise may be produced by the dynamics of particles' transfer from the minidyno chamber to the OPS detection probe. In order to synchronize the data obtained from OPS and minidyno, a novel approach was proposed. The main purpose of the proposed approach is to count the particles generated by the brake as realistically as possible. First, all the noises in the whole braking events were accurately detected and analyzed. The points with minimum number of brake emitted particles were selected as an estimate of the background noise and their standard deviation was calculated. A threshold equal to the background noise plus a standard deviation was set to select significative emission levels, i.e. not compatible with the instrument noise. Given a brake event, all the sampled points above the threshold were collected to obtain the overall emission produced, including the emission tail which follows the detachment of the pads from the disc.

### 3.2.3. Artificial neural network (ANN) emission model

ANN is an effective well-known AI-based tool that has penetrated many sciences due to its adaptivity attributes. Regarding the ability to model time-series data, these models not only are an excellent alternative to statistical models, but can also show more accurate and defensible results in investigating emission models (Moradi and Miranda-Moreno, 2020; Tuan Hoang et al., 2021). The training of a neural network is generally conducted by passing the data through the determined layers to predict the outputs and compare them with the target observations. In addition, neural networks can also have multi-layered architecture, helping them increase the chance of successfully modeling unknown phenomena (Moradi and Miranda-Moreno, 2020).

Previous studies widely investigated the efficiency of ANN algorithms in brake wear prediction. In 2010, Aleksendric developed a neural model to predict brake wears based on friction materials, sliding speed, temperature, and applied load using full-scale dynamometer data (Aleksendrić, 2010). Moreover, Hassan & Mohammad conducted an ANN model to estimate the wear rate and temperature of disc and pads based on pin-on-disc data (Hassan and Mohammed, 2016). In recent

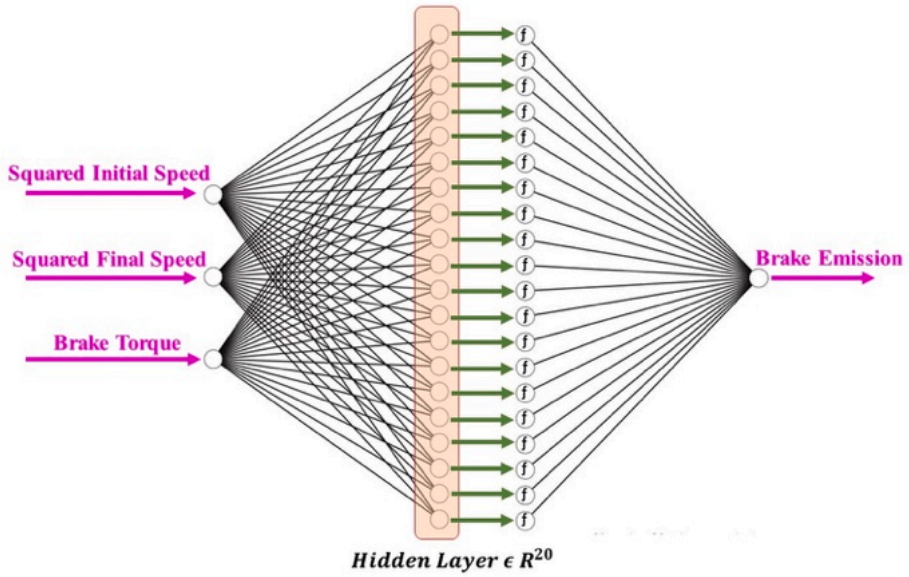


**Fig. 5.** Proposed ANN model architecture.

years, the performance of neural models in tribology has been promoted by (Argatov and Chai, 2019). Argatov and Chai introduced an ANN-supported regression model developed based on the Archard–Kragelsky model to estimate wear rate. Their model could present much lower degrees of freedom than standard ANN brake wear models. Furthermore, Vasilijevic et al. investigated the potential of the ANN model in $PM_{10}$ and $PM_{2.5}$ particle prediction emitted by the braking system (Vasiljević et al., 2022). All these studies aimed to prove the possibility of using ANN models to estimate the emission rates of the vehicle braking system, and their findings confirmed the high ability of such AI-based models in brake wear prediction.

In the present study, the research team developed a neural network model based on the data obtained by minidyno. After the integration of the signal in the time domain, the correlation between all tribological parameters and the amount of brake wear emitted was first evaluated. The square of the initial speed, in which the brake operation starts, and square of the final speed, in which the brake operation terminates, were found to be the most correlated parameters with brake wear emissions. Moreover, braking torque was also chosen regarding its correlation with brake emission generation and its influential impacts on vehicle dynamics. Aggregately, three main features were selected to feed the ANN model as a training dataset, including the square of the initial speed, the square of the final speed, and brake torque. The overall emission produced by a brake event is therefore assumed to be a function of these three independent quantities.

*3.2.3.1. Network architecture.* The first aspect that was considered in the design of the network was the choice of the input variables. We were guided by physical considerations: the amount of wear depends on the dissipated energy and on the severity of the brake event. Hence, we chose the squared initial and final velocities as the first two inputs (the difference being proportional to the dissipated energy) and the braking toque as a third input (higher braking torques, for the same dissipated energy, are likely to be more severe events). This pondered choice of the independent variables –by providing inputs that correlate with output emissions in a way as straightforward as possible– alleviates the learning burden of the network-to-be (which in turn results in higher sample efficiency, less trainable parameters, and less overfitting issues).

Hence, the neural network approximates the following function:

$$o = f\left((v_i/v_0)^2, (v_f/v_0)^2, \tau/\tau_0\right)$$

where $v_i$ and $v_f$ are the initial and final velocities, $v_0 = 50$ km/h is a convenient normalization factor (so that the input to the network is close a unity), $\tau$ is the braking torque and $\tau_0 = 1000$ Nm is the corresponding torque scaling factor.

We trained three different networks to predict the $PM_1$, $PM_{2.5}$ and $PM_{10}$ emissions by binning the corresponding minidyno channels. The output $o$ of the network was chosen as the estimated total surface area of the particles in a PM bin. The training data $\hat{o}$ for this signal were derived from the raw measured data by computing the surface area of each minidyno channel:

$$\hat{o}_{\text{bin}} = \sum_{i \in \text{binchannels}} n_i \pi (d_i)^2$$

where $n_i$ is the number of particles in the i-th channel and $d_i$ is the (mean) diameter of the particles in each channel. The summation is extended to all the channels of a PM bin.

We preferred developing a neural model that predicts the total surface area of the particles because this quantity is better correlated with the dissipated energy (this is again a physics-informed choice analogous to those above for the input). Once the total surface area is predicted, the particle number is obtained by dividing the total by the mean area of one particle of the bin. The volume (and mass) was obtained in a similar way. The alternative would have been training two different networks per bin: one predicting the particle number and another the particle volume.

The network architecture (Fig. 5) is that of a single layer perceptron. The input layer collects the three input signals and is fully connected to a hidden layer with 20 neurons, followed by Tanh activation function and fully connected to the single neuron output layer.

The size of the input layer has been chosen with few trials as a tradeoff between network descriptive capacity and risk of overfitting. With 20 neurons, the total number of parameters is 101 which is conveniently smaller than the total number of training examples (1070).

*3.2.3.2. Network supervised training.* The 1070 examples from the minidyno dataset were randomly divided into 75% for training examples (i.e. those used for stochastic gradient descent) and 25% as validation set (i.e., those used to monitor that no overfitting happens). The training process was carried out in Wolfram Mathematica with the ADAM optimizer and a batch size of 64. The monitoring of the training and validation loss functions confirmed that no overfitting happened.

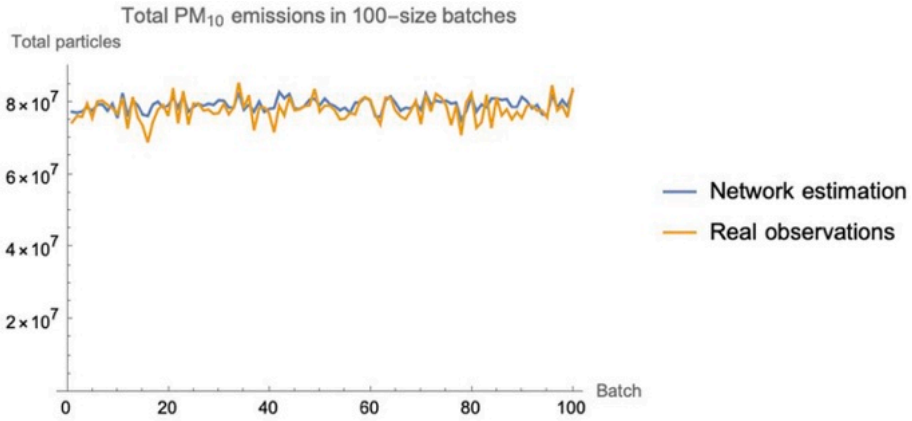


**Fig. 6.** Total emissions on batches of brake events.

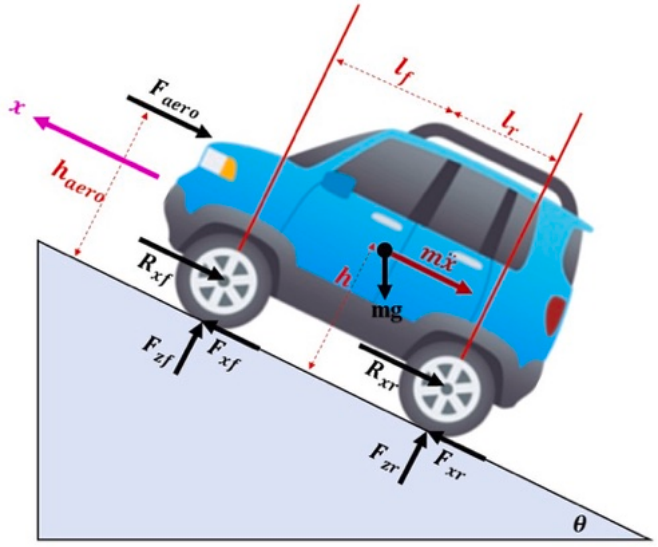


**Fig. 7.** Sketch of longitudinal dynamics forces on a vehicle.

The training was stopped after reaching a loss function plateau.

*3.2.3.3. Network performance.* The validation set was re-used as test set (because there was no overfitting, we did not save a separate test set). The coefficient of correlation ($R^2$) evaluated on the validation set was 0.88, 0.76 and 0.36, respectively for $PM_1$, $PM_{2.5}$ and $PM_{10}$. The performance apparently worsens with greater particles, because larger particles are fewer and the noise in particle count mentioned above is relatively larger.

*3.2.3.4. Residual analysis.* The residuals (network predictions minus ground-truth) in the validation set were studied finding that they were approximately iid (independent and identically distributed). This means that the difference between network prediction and observed values is an independent random noise. The network predicts the most likely value (i.e. the mathematical expectation of the emissions). However, since the variance of such noise is larger than the mean (for the $PM_{10}$ case), hence the network for $PM_{10}$ has a low ($R^2$). Nonetheless, this does not mean that the network is useless: in fact, the network predicts the most likely emission regardless of fluctuations that may be observed case by case. For a large batch of events, the random noise averages out and the network prediction of total batch emissions gets close to the total real emissions.

Indeed, we have evaluated the total emissions on random batches of 100 brake events and compared with the total of the network estimated emissions. The results are shown in Fig. 6 for $PM_{10}$ and show that when batches of 100 events are considered, the total estimated emission by the network is very close to the total observed emission. Hence, even with low ($R^2$), the network is useable for prediting the average or long-term emissions.

### 3.3. System level

#### 3.3.1. Vehicle system dynamics model

Vehicle dynamics, which is the study of vehicle motion as produced by the relevant applied actions (forces and torques), is essential to model the vehicle's real behavior at the system level (Rajamani, 2011). In normal driving conditions, the effect of the braking action involves only the longitudinal dynamics, where the translation of the vehicle suspended mass and the front and rear axles rotational dynamics are entangled. Road slope, vehicle mass and its distribution, ground coefficient of friction, brake type, radial and nominal stiffnesses of tires and other design quantities are among some parameters influencing the vehicle dynamics remarkably. In fact, these critical factors have a direct impact on the axles dynamics and the corresponding rate of emission generated by the braking system. Regardless of traffic parameters, the rate of particle generation from the braking system may vary for the front and rear axle of the vehicle. Following this approach, it is possible to analyze the traffic-related brake emissions at the resolution of the single vehicle across the transportation network, identifying relevant parameters (at system and suprasystem level) affecting the single vehicle and also the traffic overall emissions, respectively.

In the literature, the studies in which the vehicle dynamics were integrated with a traffic microsimulation model are considerably scarce. In 2018, So et al. integrated the vehicle dynamics with the VISSIM vehicle trajectories to find the exhaust emissions (So et al., 2018). In such a research, the authors inserted the VISSIM outputs into the vehicle dynamics model provided by the CarSim simulation package to use in Passenger Car and Heavy Duty Emission Model (PHEM) (Hausberger et al., 2009) to assess the emissions. This research showed that considering the integration of vehicle dynamics and traffic microsimulation models in emission estimation leads to more reliable results compared to the microsimulation-only approach. In addition, to model the behavior of autonomous and connected vehicles more realistic, Pariota et al. also implemented vehicle dynamics models besides the traffic microsimulation model simulated in SUMO regardless of vehicle emissions (Pariota et al., 2020). Their results also confirmed the reliability, functionality and added value of using vehicle dynamic model.

In the present study, since VISSIM cannot simulate the vehicle dynamics and predict the real condition of brake wear generation, a

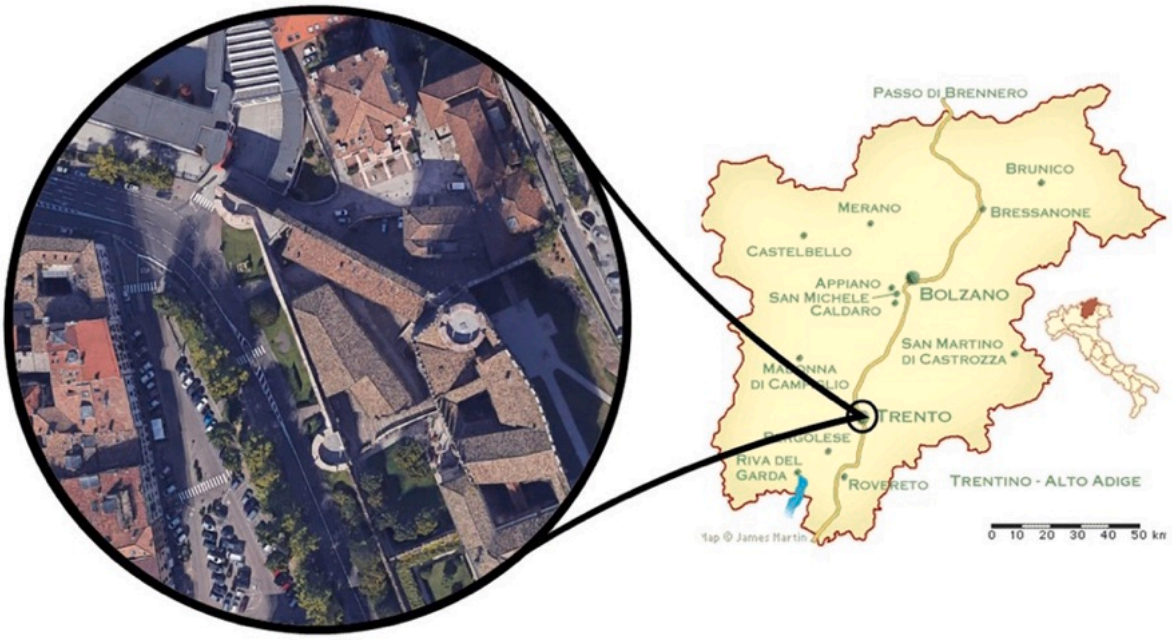


**Fig. 8.** Buonconsiglio Castle Area: Location of the studied case.

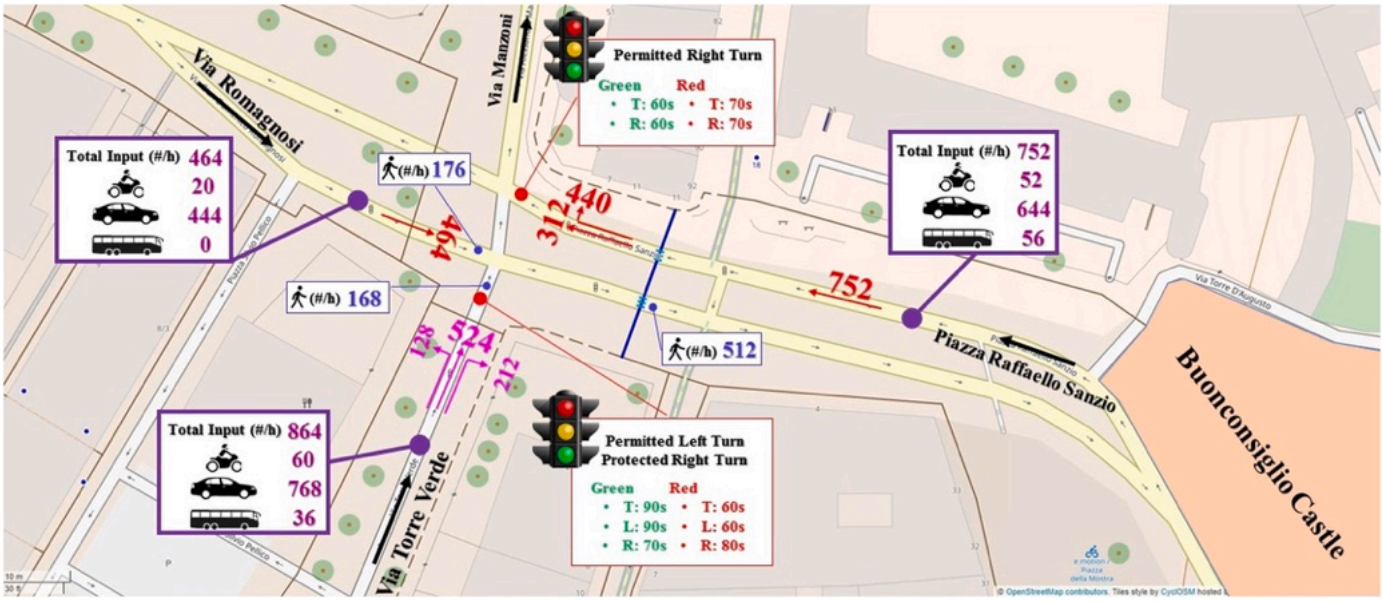


**Fig. 9.** Details of data collection in the field.

customized vehicle longitudinal dynamic model was developed in Wolfram Mathematica programming language. The model was developed by writing the symbolic equations of motion of the longitudinal dynamics of the vehicle and the wheels, subjected to the traction and resistance forces, as shown in Fig. 7. The Appendix consists of details on the model. The model was fed by the VISSIM outputs, i.e., individual trajectories and the design information of the targeted vehicle. The main concept of making this model is to calculate the vehicle's front and rear brake torques and angular velocities based on the given inputs. These outputs, together with the VISSIM outputs, are then inserted into the ANN model, previously obtained by the minidyno data, to estimate the brake emission in the case study.

### 3.4. Suprasystem level

#### 3.4.1. Case specifications

To estimate the brake wear in high-congested areas, the city center or regions near the central railway station can be a reasonable choice, where thousands of residents commute daily. The case study here investigated deals with Trento, a city on the Adige River in Trentino-Alto Adige, located in the north of Italy. A well-known castle named Buonconsiglio, located in the near city center of, was found as an appropriate location for traffic data collection. Buonconsiglio Castle is one of the city's eye-catching and stunning tourist areas, attracting thousands of tourists, commuters, citizens, and visitors annually, making its surrounding roads significantly congested in rush hours. Fig. 8 presents the case located on the map.

| Point | Direction |
|---|---|
| 1 | Two-way |
| 2 | One-way |
| 3 | Two-way |
| 4 | One-way |

| Trip | Route |
|---|---|
| 1 → 2 | A |
| 1 → 3 | B |
| 3 → 1 | C |
| 4 → 1 | D |
| 4 → 2 | E |
| 4 → 3 | F |

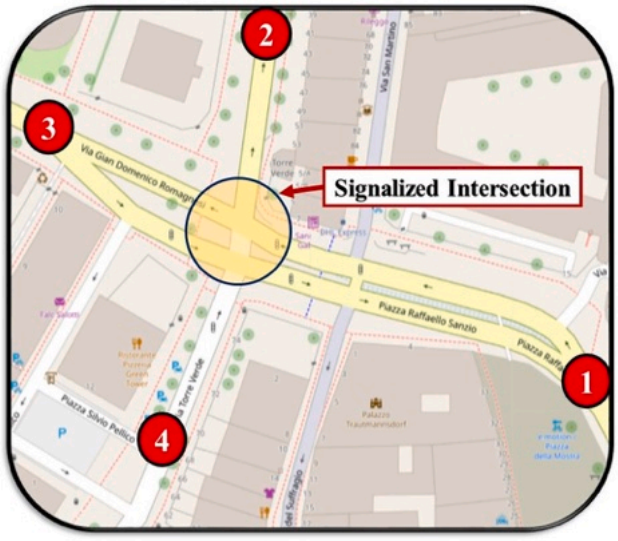


**Fig. 10.** Route definitions.

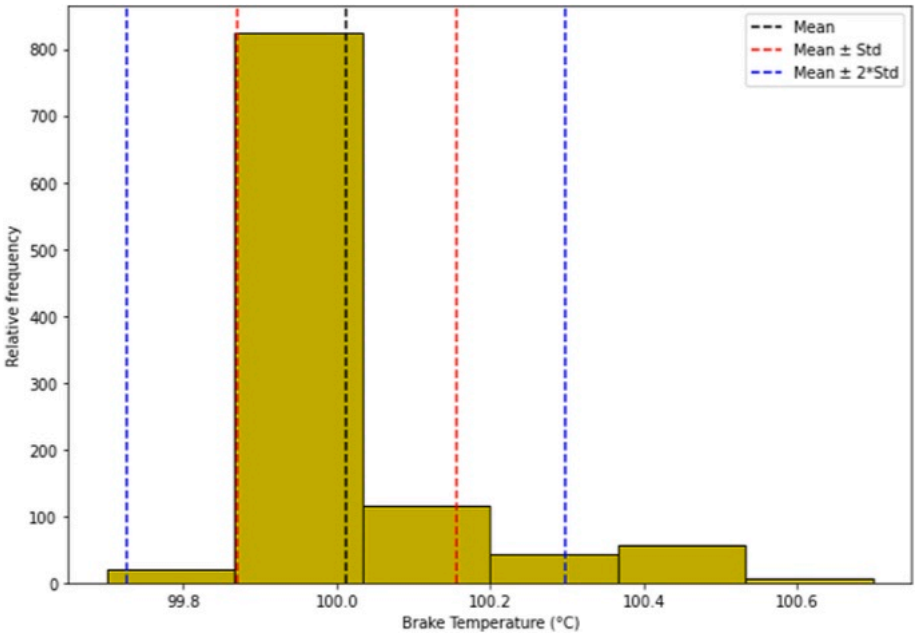


**Fig. 11.** The temperatures in the beginning of the brake events.

**Table 2**
Total number of unique targeted vehicles at each route per iteration.

| | Route A | Route B | Route C | Route D | Route E | Route F |
|---|---|---|---|---|---|---|
| Iteration 1 | 90 | 36 | 68 | 21 | 19 | 9 |
| Iteration 2 | 80 | 31 | 38 | 21 | 25 | 7 |
| Iteration 3 | 79 | 35 | 56 | 12 | 23 | 12 |
| Iteration 4 | 71 | 37 | 67 | 25 | 19 | 9 |
| Iteration 5 | 80 | 39 | 58 | 23 | 32 | 6 |
| Iteration 6 | 85 | 39 | 55 | 18 | 22 | 10 |
| Iteration 7 | 66 | 29 | 51 | 22 | 18 | 4 |
| Iteration 8 | 78 | 44 | 68 | 19 | 24 | 7 |
| Iteration 9 | 86 | 29 | 55 | 20 | 20 | 6 |
| Iteration 10 | 81 | 33 | 65 | 22 | 17 | 9 |
| **Average** | 79.6 | 35.2 | 58.1 | 20.3 | 21.9 | 7.9 |
| **STD** | 7.01 | 4.83 | 9.43 | 3.53 | 4.43 | 2.33 |

**Table 3**
Total number of brake events at each route per iteration.

| | Route A | Route B | Route C | Route D | Route E | Route F |
|---|---|---|---|---|---|---|
| Iteration 1 | 117 | 37 | 83 | 27 | 19 | 9 |
| Iteration 2 | 99 | 32 | 52 | 26 | 25 | 7 |
| Iteration 3 | 101 | 37 | 67 | 17 | 23 | 12 |
| Iteration 4 | 92 | 37 | 85 | 33 | 19 | 9 |
| Iteration 5 | 99 | 42 | 65 | 34 | 32 | 6 |
| Iteration 6 | 109 | 39 | 70 | 22 | 22 | 10 |
| Iteration 7 | 83 | 29 | 62 | 36 | 18 | 4 |
| Iteration 8 | 96 | 45 | 76 | 26 | 25 | 7 |
| Iteration 9 | 104 | 29 | 66 | 29 | 20 | 6 |
| Iteration 10 | 97 | 33 | 84 | 29 | 17 | 9 |
| **Average** | 99.7 | 36 | 71 | 27.9 | 22 | 7.9 |
| **STD** | 9.23 | 5.29 | 10.82 | 5.70 | 4.50 | 2.33 |

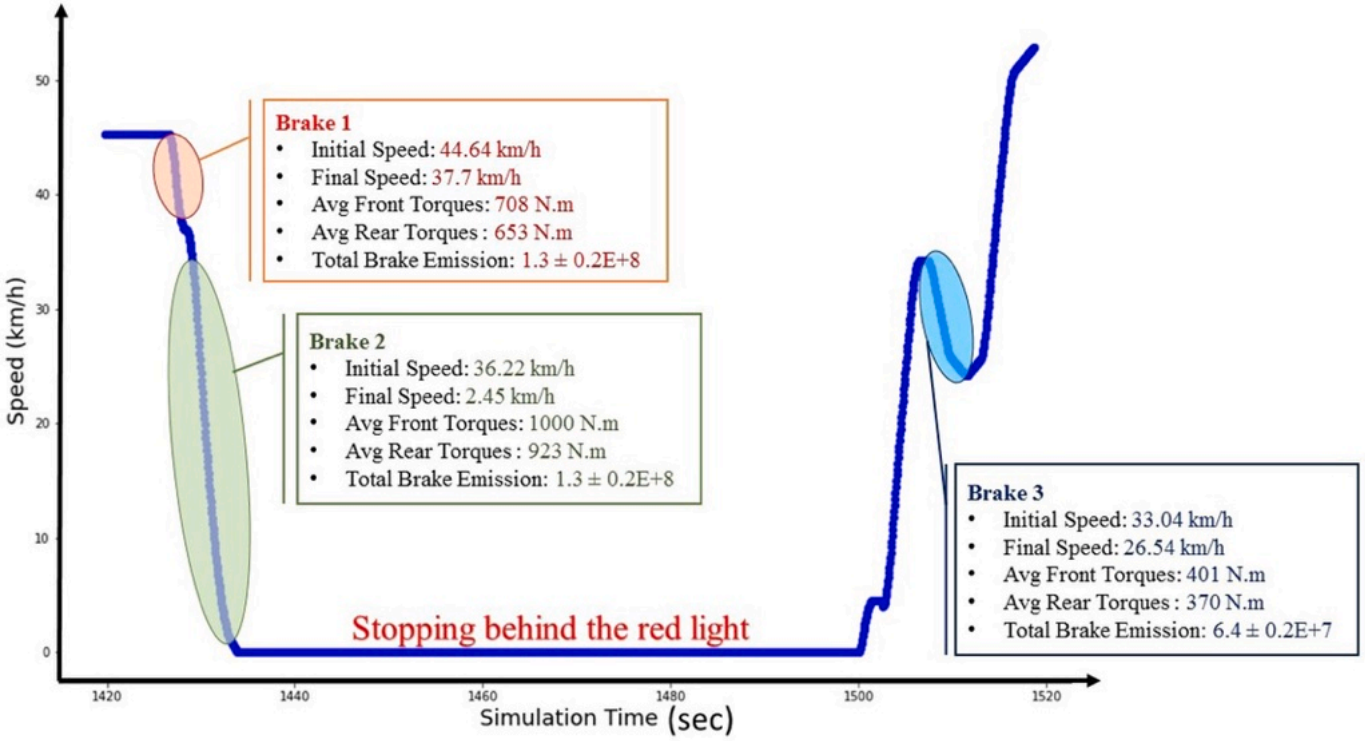


**Fig. 12.** An example of a vehicle trajectory with the number of brakes, initial and final speeds, and emitted emissions.

**Table 4**
Total number of brake particles at each route for 10 repetitions.

| | | Route A | Route B | Route C | Route D | Route E | Route F |
|---|---|---|---|---|---|---|---|
| $PM_1$ (#) | Mean | 2.28 E+10 | 9.76 E+09 | 1.32 E+10 | 3.86 E+09 | 4.40 E+09 | 1.91 E+09 |
| | STD | 1.73 E+09 | 1.19 E+09 | 2.34 E+09 | 8.97 E+08 | 1.10 E+09 | 6.63 E+08 |
| $PM_1$ (#/km) | Mean | 1.07 E+09 | 1.08 E+09 | 9.04 E+08 | 7.43 E+08 | 1.10 E+09 | 1.61 E+09 |
| | STD | 8.11 E+07 | 1.31 E+08 | 1.61 E+08 | 1.73 E+08 | 2.76 E+08 | 5.60 E+08 |
| $PM_{2.5}$ (#) | Mean | 1.85 E+09 | 7.56 E+08 | 1.04 E+09 | 3.05 E+08 | 3.38 E+08 | 1.57 E+08 |
| | STD | 1.33 E+08 | 9.11 E+07 | 1.84 E+08 | 6.99 E+07 | 8.23 E+07 | 5.66 E+07 |
| $PM_{2.5}$ (#/km) | Mean | 8.65 E+07 | 8.35 E+07 | 7.16 E+07 | 5.86 E+07 | 8.48 E+07 | 1.33 E+08 |
| | STD | 6.23 E+06 | 1.01 E+07 | 1.26 E+07 | 1.35 E+07 | 2.06 E+07 | 4.77 E+07 |
| $PM_{10}$ (#) | Mean | 1.56 E+08 | 5.87 E+07 | 9.39 E+07 | 2.90 E+07 | 2.97 E+07 | 1.25 E+07 |
| | STD | 1.04 E+07 | 6.99 E+06 | 1.62 E+07 | 6.41 E+06 | 6.50 E+06 | 4.10 E+06 |
| $PM_{10}$ (#/km) | Mean | 7.30 E+06 | 6.49 E+06 | 6.44 E+06 | 5.58 E+06 | 7.45 E+06 | 1.05 E+07 |
| | STD | 4.86 E+05 | 7.72 E+05 | 1.11 E+06 | 1.23 E+06 | 1.63 E+06 | 3.46 E+06 |

The castle's main entrance is located in a two-way street named "Via Bernardo Clesio", which ends at the Trento central railway station (500 m distance). The main traffic movements around the castle are being handled by a high-demanded four-legged signalized intersection. This intersection is located roughly close to the Castle main entrance and central railway station, which has been shaped by the cross of two highly-congested roads named Piazza Raffaello Sanzio and via Alessandro Manzoni (Via Torre Verde). Due to its strategic location, the intersection acts as the primary hub of the traffic division in the transportation network, connecting many city regions to the railway passenger terminal. Besides, numerous businesses, including minimarkets, restaurants, ice-cream stores (Gelateria), and a busy and popular store (Tabacchi shop), are located around the castle, worsening the traffic congestion in the surrounding area.

Although Trento city confronts a reasonable precipitation rate every year, air pollution is a dominant issue, especially in populated areas. However, these airborne pollutants can be originated from either exhaust or non-exhaust sources, which is still unknown. To address a solution for this problem, this research aims to estimate non-exhaust emissions focusing on brake wear generated by the dominant SUV family cars in the castle's surrounding area.

### *3.4.2. Field data collection*

The research team directly employed several Full-HD cameras to capture the movements of all agents in the network. The evening peak hour (5–6 p.m.) on a sunny day was chosen for implementing the data collection process as the highest rate of commuters could be observed in this period. The video recordings were accurately analyzed, and the route choices were determined. Traffic and non-traffic parameters, which were essential for the simulation in microlevel, were also extracted from the recordings. These parameters included vehicles input volume, modal splits, desired speeds, signal timings, number of pedestrians at each side, number of parking lots, number of lanes for each road, roads geometry, intersection characteristics, and agents conflict areas. Fig. 9 shows the data collection in the case field in detail. In this figure, all units are in "per hour" except the traffic lights, which have the "second" unit. In contrast to the other roads, the right turn movement of Via Torre Verde was found protected with different green and red timings.

**Table 5**
Total mass of brake particles at each route for 10 repetitions.

| | | Route A | Route B | Route C | Route D | Route E | Route F |
|---|---|---|---|---|---|---|---|
| $PM_1$ (mg) | Mean | 1.00 E+00 | 4.29E-01 | 5.80E-01 | 1.70E-01 | 1.94E-01 | 8.42E-02 |
| | STD | 7.62E-02 | 5.23E-02 | 1.03E-01 | 3.95E-02 | 4.84E-02 | 2.92E-02 |
| $PM_1$ (mg/km) | Mean | 4.71E-02 | 4.75E-02 | 3.98E-02 | 3.27E-02 | 4.86E-02 | 7.11E-02 |
| | STD | 3.57E-03 | 5.78E-03 | 7.07E-03 | 7.59E-03 | 1.22E-02 | 2.46E-02 |
| $PM_{2.5}$ (mg) | Mean | 1.92 E+00 | 7.87E-01 | 1.09 E+00 | 3.17E-01 | 3.52E-01 | 1.64E-01 |
| | STD | 1.38E-01 | 9.49E-02 | 1.92E-01 | 7.28E-02 | 8.57E-02 | 5.89E-02 |
| $PM_{2.5}$ (mg/km) | Mean | 9.01E-02 | 8.70E-02 | 7.45E-02 | 6.10E-02 | 8.83E-02 | 1.38E-01 |
| | STD | 6.49E-03 | 1.05E-02 | 1.32E-02 | 1.40E-02 | 2.15E-02 | 4.97E-02 |
| $PM_{10}$ (mg) | Mean | 2.06 E+00 | 7.77E-01 | 1.24 E+00 | 3.84E-01 | 3.93E-01 | 1.65E-01 |
| | STD | 1.37E-01 | 9.25E-02 | 2.14E-01 | 8.48E-02 | 8.61E-02 | 5.42E-02 |
| $PM_{10}$ (mg/km) | Mean | 9.66E-02 | 8.59E-02 | 8.52E-02 | 7.38E-02 | 9.85E-02 | 1.39E-01 |
| | STD | 6.44E-03 | 1.02E-02 | 1.47E-02 | 1.63E-02 | 2.16E-02 | 4.57E-02 |

### 3.4.3. Traffic microsimulation

In the last decade, traffic microsimulation models have been widely used to develop vehicle movement and activity data to predict the exhaust emissions in urban areas as vehicle-based environmental issues are becoming more severe daily. Traffic microsimulation software is a versatile tool providing a systematic approach to depicting individual records. PTV-VISSIM, developed by PTV-Group, is a well-known and reliable microsimulation package that can provide the agents' driving conditions based on the user attributes. Previous studies introduced VISSIM as an authentic software for monitoring individuals' traffic parameters like speed, acceleration, travel time, and delay based on vehicle trajectories (Y. Chen et al., 2021; Hirschmann et al., 2010). Jie et al. also confirmed the accuracy of speed and acceleration distributions provided by VISSIM using a local Sensitivity Analysis method (Jie et al., 2013; Song et al., 2020).

VISSIM is capable of estimating exhaust emissions in the nodes defined by the user throughout the network. However, currently, there is no evidence of using traffic microsimulation models to predict non-exhaust emissions. Some studies implemented the default emission model previously embedded in VISSIM to estimate exhaust emissions in different traffic conditions. The emission data used in the VISSIM default exhaust emission model was provided by the Oak Ridge National Laboratory of the U.S. Department of Energy, as well as the standard formulas extracted from TRANSYT 7-F, a program for optimizing signal times (PTV Group, 2022). Alvanchi et al. used the VISSIM default emission model to calculate exhaust emissions throughout the construction period of a grade separation located near sensitive locations (Alvanchi et al., 2019, 2020). The performance of the VISSIM default emission model was also evaluated in a port city surrounded by several freeways to investigate the impacts of heavy goods vehicles on air pollution (Rahimi et al., 2022; Ziemska, 2021). Although the default emission model can be used to evaluate the emission in nodes, it is unable to provide the emissions generated by agents in time-series. On the other hand, some previous studies have focused on using vehicle second-by-second records provided by VISSIM. These records were used as inputs for feeding other pre-determined exhaust emission models, such as emission models associated with agents' speed profiles (Salamati et al., 2015), Environmental Protection Agency's MOVES (Motor Vehicle Emission Simulator) emission model (Abou-Senna et al., 2013; Abou-Senna and Radwan, 2013; Gu et al., 2018; Karabag et al., 2020), Passenger car and Heavy-duty Emission Mode (PHEM) (Hirschmann et al., 2010; Kraschl-Hirschmann et al., 2011), and Comprehensive Modal Emission Model (CMEM) (K. Chen and Yu, 2007; Noland and Quddus, 2006; Stevanovic et al., 2009).

Although all these previous studies have focused on estimating exhaust emissions using traffic microsimulation, no previous work can be found in the literature in which non-exhaust emissions were estimated based on traffic simulation-based approaches. The reason may be related to the challenges of synchronization between suprasystem, system and subsystem levels. The brake wear behaviors can be investigated at the subsystem level, while traffic microsimulation models can record the vehicle movements at the suprasystem level. Basically, this synchronization cannot be done unless an interdisciplinary approach is employed. The approach can connect various sciences, i.e., transportation engineering, mechatronics and mechanical engineering, environmental impact assessment, and computer science. The present research aims to estimate brake emission generated by the dominant vehicles while braking operation in urban area by implementing traffic microsimulation models, vehicle system dynamics, tribological tests, and ML-based ANN algorithms.

*3.4.3.1. Simulation parameters.* Some traffic network information is essential for the VISSIM to make the simulation model. This information includes vehicle and pedestrian volumes, vehicle types (Light-vehicle (LV) and Heavy-vehicle (HV)), signal configurations, timings, and roads geometry. However, other elements may also be provided based on the project's needs. For the simulation model, firstly, the design information of the targeted vehicle was embedded in the software to ensure considering the ground-truth data. The hourly number of pedestrians was also applied to the simulation model collected in the field survey regardless of their gender. Also, exclusive sidewalks and signalized crosswalks were designed for all the pedestrians in the network to avoid interfering vehicle movements. Based on the observations in the field, all pedestrian signals were configured as protected signal timings for all signalized crosswalks.

In VISSIM, the simulated model releases the input vehicles stochastically in the network, originating from Wiedemann's car-following model (PTV Group, 2022). To meet the statistical analysis needs, the 1-h simulation model was run ten times with the resolution of 20 time-steps per simulation second (a record at each 0.05 s) with 42 random seeds. Therefore, the simulation model conducted more than 26 million records in total.

To use the individuals' records in the vehicle dynamics and ANN model, all the necessary activity information at each timestamp was extracted from the simulation results. This information includes agents' speed, acceleration, coordination, type, model, number, height, length, width, lane state, position, and driving state in the network. Then, the average emission among ten simulation iterations of each defined route was calculated, and lastly, the results were reported and concluded.

### 3.4.4. Data preparation

Within 26 million total records, first, the records of all targeted vehicles were extracted from the VISSIM output for all simulation runs. On average, almost 650,000 records of targeted vehicles were observed at each simulation run, which was approximately 7 million records in all ten simulation repetitions. Based on the vehicles' trajectories, six separate routes were defined in the network consisting of all the motorway roads around the castle. Fig. 10 shows the defined routes in detail.

For each repetition, the individuals' driving behaviors were scrutinized after finding the trajectories of the vehicles. Behaviors consisted of the driving state, number of brakes, brake durations, speed, and deceleration (i.e. intensity) during brake event operated in the vehicle trajectory. All this brake-related information was then fed into the vehicle dynamics model to calculate the front and rear braking torques. After finding the average of the front and rear torques for each braking event,

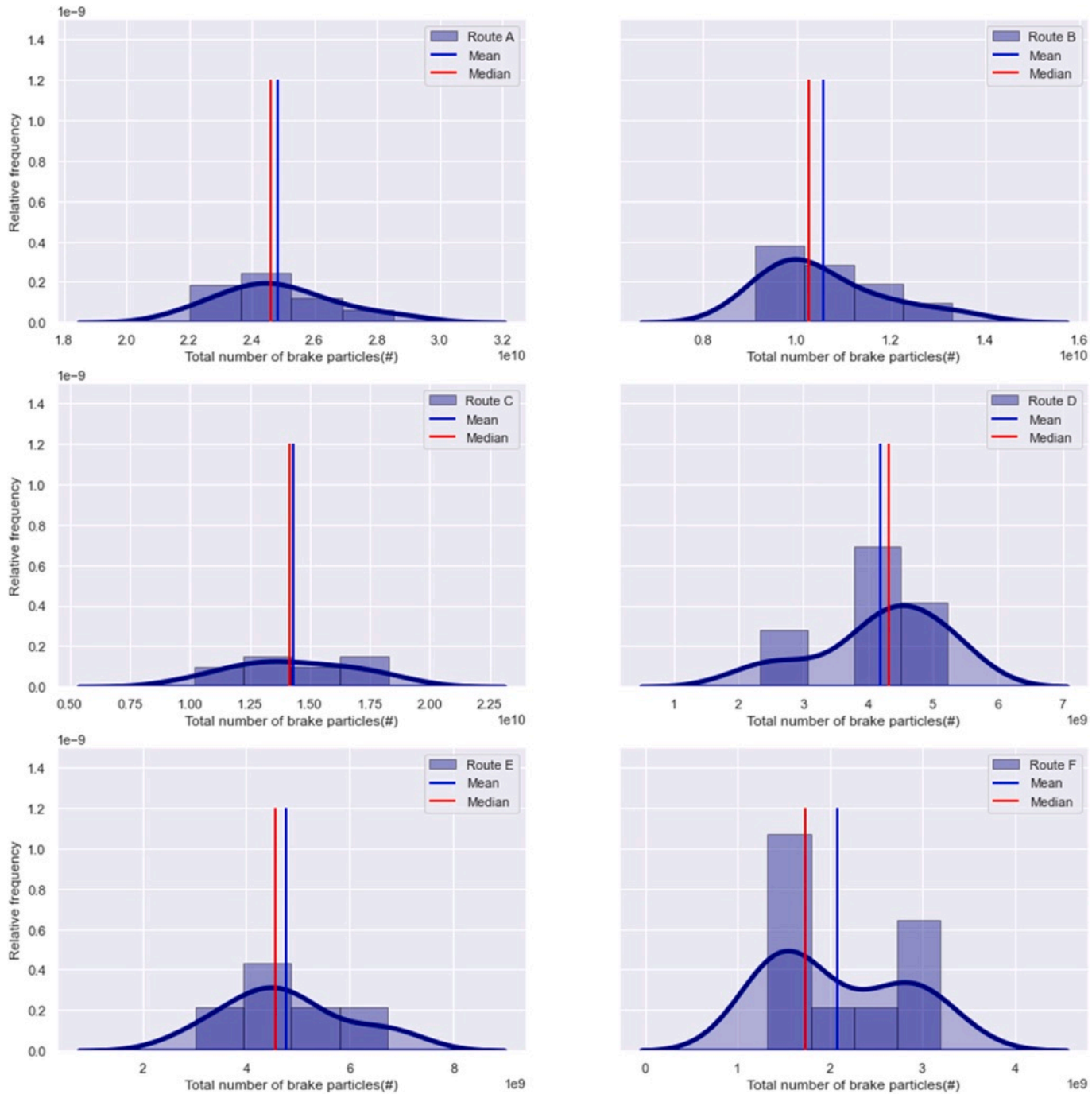


**Fig. 13.** Kernel Density estimation of PN brake emissions for each route.

the initial and final speeds of every brake of each targeted vehicle were added to the average torques to shape the main data frame. Next, the data frame was inserted into the ANN model to estimate the emission produced by every brake event. The total emissions generated by each vehicle in a particular route were calculated by summating the obtained number of particles for all brake events per vehicle.

## 4. Results and discussion

### 4.1. Brake temperature configurations

The braking system struggles with the varying temperatures of the brake pads and discs during braking. The friction between the disc and the pads increases the braking temperature considerably. However, once the braking process is complete, the temperature begins to drop due to air circulation. At the beginning of the braking process, the minidyno machine must be warmed up and several run-in braking cycles are performed to create the steady state conditions for the tests, which in turn ensure the steady state working temperature of the braking system. The braking parameters were chosen to prevent disc temperature from exceeding approx. 150 °C. This temperature is the maximum disc temperature generally admitted in the WLTP brake cycle (Mathissen et al., 2018). This temperature represents the typical transition temperature for brake materials. Above this temperature, the PN number can change by orders of magnitude due to the sharp increase in the ultrafine fraction (Alemani et al., 2016). For this purpose, a threshold temperature

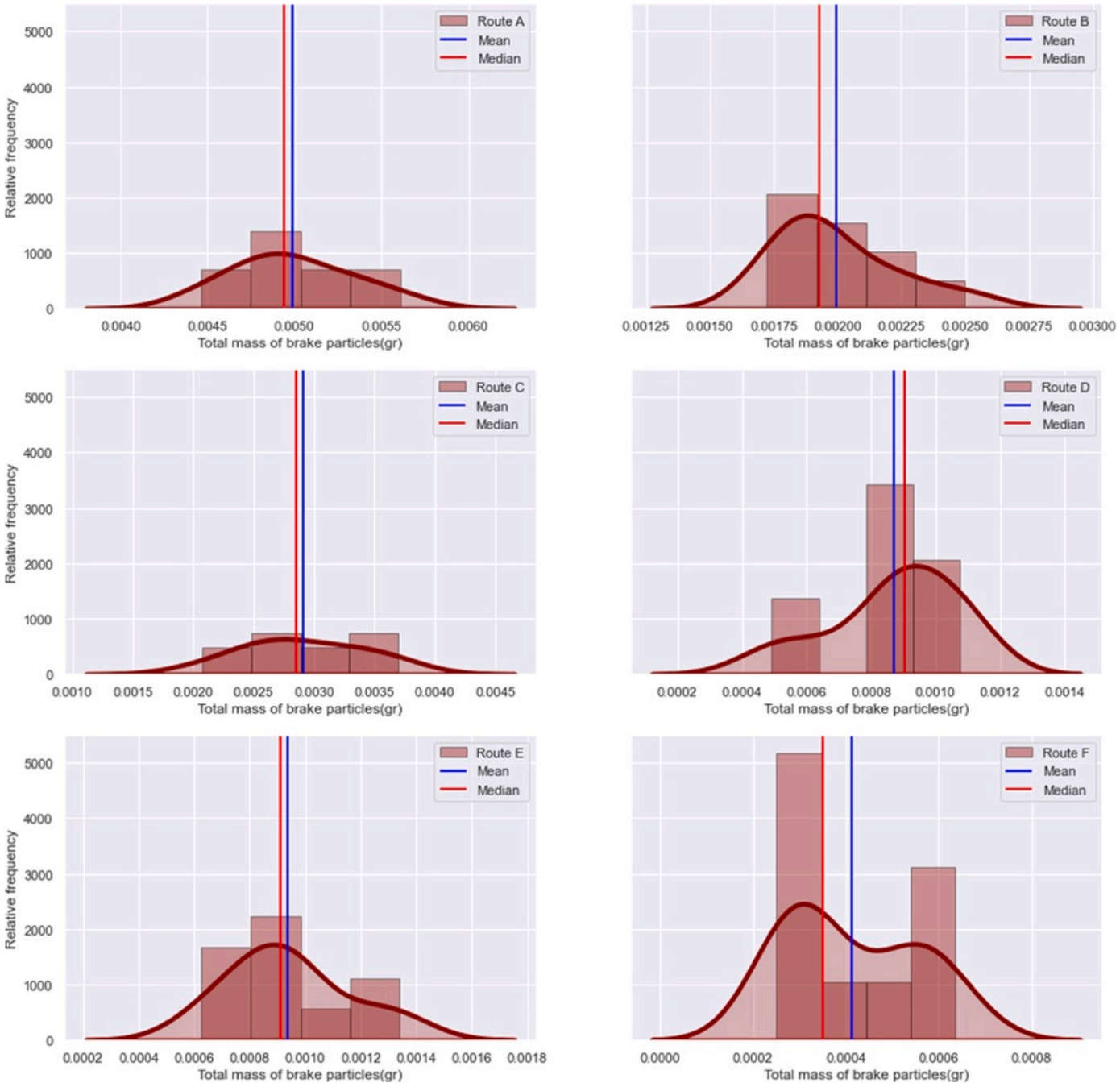


**Fig. 14.** Kernel Density estimation of brake particle mass for each route.

(100 °C) was set for the machine as the starting time of the braking events, at which the next braking event should start among more than 1000 tests. The temperature of 100 °C was chosen to avoid exceeding the transition temperature and allow a reasonable duration of the test, since the cooling of the system decreases with temperature. In addition, the temperatures below 100 °C was not considered in the study because it did not expose influential impacts, as shown in a recent study (Men et al., 2022). Fig. 11 shows the temperatures at the beginning of the braking operations and their relative frequency during all braking operations.

### 4.2. Total number of unique targeted vehicles

Every targeted vehicle may experience different driving conditions during its trip, causing the implementation of numerous brake events. In the case of red light signal observation, drivers may use either continuous or intermittent brake operation, which increases the braking system temperature releasing the brake particles. To estimate the produced emissions at each determined route, first, the total number of unique targeted vehicles were calculated, which is presented in Table 2.

### 4.3. Total number of brake events

In the case study, all the moving information of targeted vehicles was extracted from the whole microsimulation dataset. Having a congested signalized intersection in front of the castle with pretimed timing configurations remarkably affected the number of brake events in the network. Brake events were different in terms of duration, initial speed,

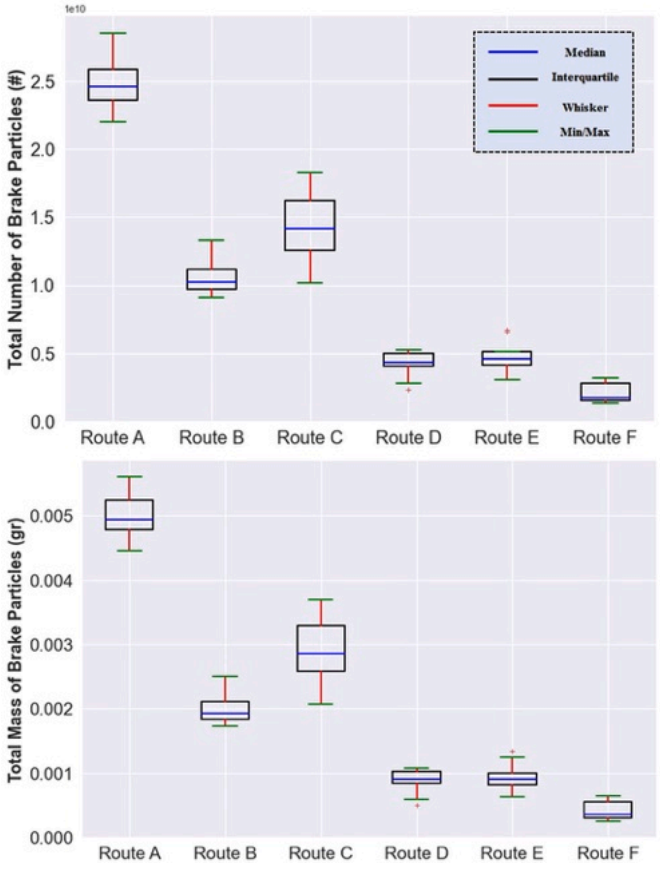


**Fig. 15.** Box plot of the total brake emissions per route in terms of PN and mass based on the KDE distributions.

final speed, and deceleration. In the proposed method, all incomplete brake events throughout the whole individuals' trajectories were dropped from the total brakes. Furthermore, the brake events with intangible velocity drops ($\Delta V < 5\ km/h$) were also neglected. The total number of accepted brake events at each route is presented in Table 3.

An example of the velocity time history of a vehicle in the simulation model is presented in Fig. 12.

The uncertainties of the ANN model's predictions are determined by the emission measurement uncertainty used to train it and by the network accuracy, where the former constitutes the dominant contribution. Typical values of the prediction uncertainty are on the order of $10^6$ particles/brake, resulting negligible with respect to the standard deviations of the overall emission obtained by repeating the traffic simulation (on the order of $10^8$ particles). The repetition of the traffic simulation is therefore assumed as the main source of dispersion of the emission estimations.

### 4.4. Total number and mass of generated brake wear particles at each route

The proposed method was successfully conducted in the case study, and the particle number and the particle mass generated by the targeted vehicles in the transportation network was calculated. Table 4 and Table 5 represent the total particle number and total particle mass, in terms of their sizes, achieved in 10 simulation repetitions at each defined route, respectively. These tables include the mean and standard deviation of the obtained results regarding the particles' diameters ($PM_1$, $PM_{2.5}$, and $PM_{10}$). All these results were calculated based on the number of brake events and brake duration that each targeted vehicle experienced through its journey.

As shown in Tables 4 and 5, the targeted vehicles commuting on Route A totally generated the highest PNs and particles' mass in all PM categories. As expected, compared to the other PM classes, $PM_1$ contributed the highest proportion of PN and mass generation with an average of 2.28 E+10 number of particles and 1.00 E-03 g of mass in the peak hour, respectively. However, considering the length of each route, the vehicles in Route F generated the highest proportion of brake emissions per 1 km travel distance regarding the extensive numbers of brake events per vehicle in this route.

To better understanding of the density distribution among the iterations route-by-route, the Kernel Density Estimator (KDE) was employed on the overall PN and particle mass. Fig. 13 represents the Kernel Density estimation of brake wear emissions (in terms of PN and particle mass regardless of the particle size) for each route over histograms of results to determine the distribution shape better and have a continuous distribution view.

As shown in Figs. 13 and 14, the concentrations of results in Routes A, C, and E are reasonably concentrated in the middle of intervals. This is related to the fair equality of means and medians over the results obtained for each route. However, Route D showed a right-skewed density curve meaning that the median is greater than the mean. Moreover, all the KDE distributions, except Route F, only had one peak, which can be described as unimodal distributions. To compare the medians and distributional characteristics of each route, box plots were drawn in Fig. 15.

As shown in Fig. 15, Route A demonstrated the highest total number of emitted brake particles regardless of the routes' length. Moreover, the box plots of all routes except Route A and C are relatively condensed, meaning that the results in these routes vary less (are more consistent). Nevertheless, Route C shows a much larger width of the box plot making the median to be off by quite a bit. Thus, Route B, D, E, and F with a more consistent total number of brake wear particles should make predictions more dependable than the more variable Route A and C results. The vehicles in the Routes D and E, which originated from Alessandro Manzoni (Via Torre Verde) road, have kind of equal medians representing a relatively equal number of emitted brake wear particles.

### 4.5. Total number and mass of generated brake wear particles in the whole network

Aggregation of brake wear particles emitted by the targeted vehicles in all routes can significantly influence the air quality in the whole transportation network. Fig. 16 illustrates the total PN and particle mass generated by all the targeted vehicles existing in the network.

In Fig. 16, the x-axis represents the total particle number (#) and particle mass (gram), and the y-axis shows the relative frequency. The total number of brake wear emissions for the 6.44 E+10 interval occurs four times out of 10 iterations. Thus, it has a relative frequency of 40% in the whole emission results. While the total emissions for the 5.76 E+10 and 6.17 E+10 intervals demonstrated the minimum frequency among all repetitions. Furthermore, the total brake wear mass for the 0.0128gr interval occurs five times out of 10 iterations. Thus, it has a relative frequency of 50% in the whole mass results.

## 5. Conclusion

This study presents a novel approach for estimating generated brake wear in urban areas. Previous studies have widely used traffic microsimulation models for exhaust emission prediction. However, no previous research has regarded the implementation of these models in non-exhaust emission estimation. The present research's primary goal is to fill this gap in the literature by proposing an innovative simulation-based approach using a vehicle dynamics model and machine learning algorithms. For this purpose, the number of particles and their masses generated by the braking system of targeted vehicles in different urban routes in a real case study were estimated. To gain this goal, a combination of suprasystem, system and subsystem investigation levels was

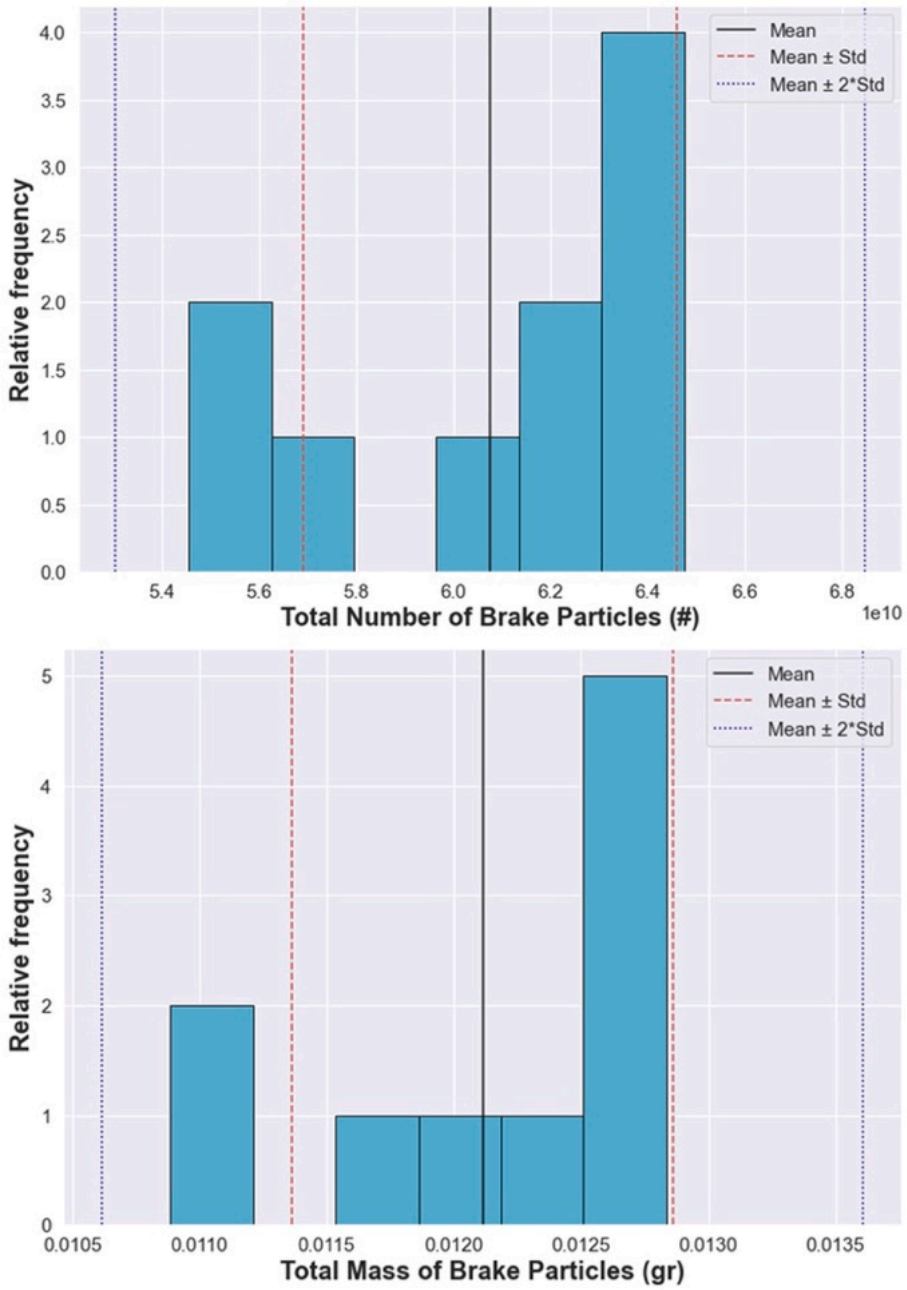


**Fig. 16.** Total PN and particle mass in the whole transportation network.

implemented. The brake wear estimation in a real area can provide supplementary information to the environmental decision-makers to earn better insight into the rate of non-exhaust emissions generation besides the exhaust emissions. The proposed method was successfully applied to the case study of a transportation network surrounding a well-known castle in Trento, Italy, using a traffic simulation package available in the market, a vehicle dynamics model, a reduced-scale dynamometer, and a neural network model.

To calculate number of emitted brake wear and the particle mass, an SUV family car was chosen as the targeted vehicle, and different available vehicle route decisions were defined based on the field survey. Results achieved in the case study represented the existing deviations in the generation of total brake PNs and masses in terms of route decisions and simulation repetitions. The total brake PN and mass in the whole transportation network also demonstrated fairly smooth differences in terms of iterations. The results showed that the routes and trajectories chosen by agents can have remarkable differences in the number of particles they produce (on the order of billions of particles) and brake particle mass in the travel distance. These route decisions can affect the number of braking events, especially in metropolitan areas where there are many commuters and the number of signalized intersections is relatively high.

Considering both subsystem level, in which the brake wear particles are investigated regarding the tribological behaviors, and system/suprasystem levels, in which vehicles' activities can be simulated at the microscopic level, to calculate the number of generated brake wear and their mass in urban areas is proposed for the first time in this research. For future work, the authors recommend the use of a fate/dispersion model for brake particle assessment. Additionally, the brake emission modelling (PM estimations) can be improved by using data from an actual full-scale dynamometer setup that complies with current global technical regulation (GTR) on brake wear particle emission

measurements. Moreover, evaluating the whole particle range including ultrafine particles and considering brake temperatures can further develop the brake emission model proposed in this research. Similar brake emission estimation is also recommended for other types of congested locations such as stop-sign intersections, semi-actuated and actuated signalized intersections, and bus terminals. By following the proposed method for such congested areas, where a remarkable number of brake events may happen, the environmental engineers and decision-makers can prevent the adverse impacts of brake wear particles on the susceptible groups of commuters, tourists, residents, and citizens living or commuting around the location.

It is worth mentioning that the conclusions are made based on our observations made by tribological tests and the results obtained by traffic microsimulation in our case study. For further investigation in future works, we are enthusiastic about exploring the results of our proposed method in other cases with totally different traffic behaviors and various geometries (different curvature and inclination), even in different weather conditions.

## Author contributions

The authors confirm contribution to the paper as follows: Conceptualization, investigation, resources, literature review, traffic simulation, traffic microsimulation modeling, field data collection, data curation, data filtration, visualization, data analysis, original draft preparation, final draft preparation & revisions: **Rahimi, M.**; Analysis and interpretation of results: **Rahimi, M.**, **Bortoluzzi, D.**; Tribological tests by minidyno: **Candeo, S.**; Methodology, supervision, final draft revisions: **Bortoluzzi, D.**; ANN brake emission model: **Da Lio, M., Bortoluzzi, D.**; Longitudinal vehicle dynamics model: **Bortoluzzi, D., Biral, F.**; Targeted vehicle information: **Biral, F.**; Project administration: **Bortoluzzi, D., Wahlström, J.**; Reviewing and editing the manuscript: **Rahimi, M., Bortoluzzi, D., Biral, F., Wahlström, J., Candeo, S., Da Lio, M.**; All authors have read and agreed to the published version of the manuscript.

## Funding

The research performed at the University of Trento is funded by the Italian Ministry for Education, University, and Research under the program Department of Excellence 2018–2022. The research performed at Lund University is funded by the European Union's Horizon 2020 research and innovation programme under grant agreement No. 954377 (nPETS project).

## Declaration of competing interest

The authors declare that they have no known competing financial interests or personal relationships that could have appeared to influence the work reported in this paper.

## Acknowledgements

We deeply thank to PTV-Group company for providing the full-license of the last version of PTV-VISSIM traffic microsimulation software.

## Appendix. Vehicle Longitudinal Dynamics Model

The vehicle longitudinal dynamic model here described assumes that no limit conditions are reached by the tyres, making it possible to adopt linear models for the tyres' forces and torques.

Referring to Fig. 7, we write the Newton's equation of the vehicle projected along the longitudinal direction of the vehicle (x):

$$m\,\ddot{x} = F_{xf} + F_{xr} - R_{xf} - R_{xr} - F_{aero} - mg\sin(\vartheta) \quad \text{(Eq. 1)}$$

where:

- $m$→ vehicle mass
- $\ddot{x}$→ vehicle acceleration
- $F_{aero}$→ aerodynamic drag force
  - $F_{xf}$→ longitudinal force of front tire
  - $F_{xr}$→ longitudinal force of rear tire
  - $R_{xf}$→ front tires rolling resistance force
  - $R_{xr}$→ rear tires rolling resistance force
  - $g$→ gravity acceleration
- $\vartheta$→ road slope

The resistances are estimated as follows:

$$R_{xf} = f\,F_{zf} \quad \text{(Eq. 2)}$$

$$R_{xr} = f\,F_{zr} \quad \text{(Eq. 3)}$$

$$F_{aero} = \frac{1}{2}\rho\,C_w A\,\dot{x}^2 \quad \text{(Eq. 4)}$$

where:

- $f$→ rolling resistance coefficient
- $F_{zf}$→ normal force on front tire
- $F_{zr}$→ normal force on rear tire
  - $\rho$→ air mass density
  - $C_w$→ aerodynamic drag coefficient

- $A$→ vehicle frontal area
- $\dot{x}$→ vehicle speed

Projecting the Euler's equation in the moving frame, we can calculate the normal forces on the front and rear tyres assuming that the vehicle pitch acceleration is negligible:

$$F_{zf} = \frac{1}{l_f + l_r}(-F_{aero}h_{aero} - m\,\ddot{x}\,h - mghsin(\vartheta) + mgl_r\,cos(\vartheta)) \quad \text{(Eq. 5)}$$

$$F_{zr} = \frac{1}{l_f + l_r}\left(F_{aero}h_{aero} + m\,\ddot{x}\,h + mghsin(\vartheta) + mgl_f\,cos(\vartheta)\right) \quad \text{(Eq. 6)}$$

where:

- $l_f$→ longitudinal distance between front axle and center of mass
- $l_r$→ longitudinal distance between rear axle and center of mass
- $h_{aero}$→ height of aerodynamic drag force
- $h$→ center of mass height

The tyre longitudinal forces are assumed to be proportional to the longitudinal slip and the normal forces:

$$F_{xf} = K_f\sigma_f \quad \text{(Eq. 7)}$$

$$F_{xr} = K_r\sigma_r \quad \text{(Eq. 8)}$$

where:

- $K_f$→ front tire longitudinal stiffness [N/slip unit]
- $K_r$→ rear tire longitudinal stiffness [N/slip unit]
- $\sigma_f$→ front longitudinal slip ratio
- $\sigma_r$→ rear longitudinal slip ratio

Where the front and rear slip ratios are defined as follows:

$$\sigma_f = \frac{r_{ef}\omega_f - \dot{x}}{\dot{x}} \quad \text{(Eq. 9)}$$

$$\sigma_r = \frac{r_{er}\omega_r - \dot{x}}{\dot{x}} \quad \text{(Eq. 10)}$$

where:

- $\omega_f$→ front wheel angular velocity
- $\omega_r$→ rear wheel angular velocity
- $r_{ef}$→ front wheel effective radius
- $r_{er}$→ rear wheel effective radius

The effective radius are:

$$r_{ef} = r_0 - \frac{F_{zf}}{k_t} \quad \text{(Eq. 11)}$$

$$r_{er} = r_0 - \frac{F_{zr}}{k_t} \quad \text{(Eq. 12)}$$

where:

- $r_0$→ undeformed tire radius
- $k_t$→ vertical tire stiffness

The wheels' dynamics is described by the two Euler equations:

$$J_f\dot{\omega}_f = -F_{xf}r_{ef} - T_f - T_{rf} \quad \text{(Eq. 13)}$$

$$J_r\dot{\omega}_r = -F_{xr}r_{er} - T_r - T_{rr} \quad \text{(Eq. 14)}$$

where:

- $\dot{\omega}_f \rightarrow$ front wheel angular acceleration
  - $\dot{\omega}_r \rightarrow$ rear wheel angular acceleration
- $J_f \rightarrow$ front wheel inertia
  - $J_r \rightarrow$ rear wheel inertia
  - $T_f \rightarrow$ front braking torque
- $T_r \rightarrow$ rear braking torque
  - $T_{rf} \rightarrow$ front wheel resistance torque
- $T_{rr} \rightarrow$ rear wheel resistance torque

We assume hereinafter that the braking system is tuned to provide a pre-defined front/rear braking torque partition:

$$T_f = k_b T \quad \text{(Eq. 15)}$$

$$T_r = (1 - k_b) T \quad \text{(Eq. 16)}$$

where:

- $k_b \rightarrow$ brake distribution coefficient

The resistance torques are given by:

$$T_{rf} = fr_{ef} F_{zf} \quad \text{(Eq. 17)}$$

$$T_{rr} = fr_{er} F_{zr} \quad \text{(Eq. 18)}$$

The inverse dynamics model is found by means of the following steps. The tyres' slip equations (9) and (10) are solved for the angular velocities, which are substituted into the wheels' Euler equations together with the tyres' normal and longitudinal forces. The two equations are then solved for the tyres' slip, which result functions of the vehicle acceleration. The calculated forces are substituted into the Newton's equation, which is solved for the total braking torque T, yielding $T_f$ and $T_r$ as functions of the vehicle acceleration. The wheels' angular velocities are calculated by means of the tyres' slip and vehicle velocity, according to equations (9) and (10). The final set of four equations (two torques and two angular velocities) constitute and inverse dynamics algebraic model: given the vehicle motion (acceleration time history) it provides the relevant quantities.

## References


Abou-Senna, H., Radwan, E., 2013. VISSIM/MOVES integration to investigate the effect of major key parameters on CO2 emissions. Trans. Res. Part D Trans. Environ. 21 https://doi.org/10.1016/j.trd.2013.02.003.

Abou-Senna, H., Radwan, E., Westerlund, K., Cooper, C.D., 2013. Using a traffic simulation model (VISSIM) with an emissions model (MOVES) to predict emissions from vehicles on a limited-access highway. J. Air Waste Manag. Assoc. 63 (7) https://doi.org/10.1080/10962247.2013.795918.

Agudelo, C., Vedula, R.T., Odom, T., 2018. Estimation of transport efficiency for brake emissions using inertia dynamometer testing. SAE Technical Papers. https://doi.org/10.4271/2018-01-1886.

Aleksendrić, D., 2010. Neural network prediction of brake friction materials wear. Wear. https://doi.org/10.1016/j.wear.2009.07.006.

Alemani, M., Nosko, O., Metinoz, I., Olofsson, U., 2016. A study on emission of airborne wear particles from car brake friction pairs. SAE Int. J. Mater. Manuf. https://doi.org/10.4271/2015-01-2665.

Alnaqi, A.A., Barton, D.C., Brooks, P.C., 2015. Reduced scale thermal characterization of automotive disc brake. Appl. Therm. Eng. https://doi.org/10.1016/j.applthermaleng.2014.10.001.

Alvanchi, A., Rahimi, M., Alikhani, H., 2019. Air pollution concentration near sensitive urban locations: a missing factor to consider in the grade separation projects. J. Clean. Prod. 228 https://doi.org/10.1016/j.jclepro.2019.04.300.

Alvanchi, A., Rahimi, M., Mousavi, M., Alikhani, H., 2020. Construction schedule, an influential factor on air pollution in urban infrastructure projects. J. Clean. Prod. 255, 120222 https://doi.org/10.1016/j.jclepro.2020.120222.

Amato, F., Cassee, F.R., Denier van der Gon, H.A.C., Gehrig, R., Gustafsson, M., Hafner, W., Harrison, R.M., Jozwicka, M., Kelly, F.J., Moreno, T., Prevot, A.S.H., Schaap, M., Sunyer, J., Querol, X., 2014. Urban air quality: the challenge of traffic non-exhaust emissions. J. Hazard Mater. 275, 31–36. https://doi.org/10.1016/j.jhazmat.2014.04.053.

Argatov, I.I., Chai, Y.S., 2019. An artificial neural network supported regression model for wear rate. Tribol. Int. 138 https://doi.org/10.1016/j.triboint.2019.05.040.

Bondorf, L., Köhler, L., Grein, T., Epple, F., Philipps, F., Aigner, M., Schripp, T., 2023. Airborne brake wear emissions from a battery electric vehicle. Atmosphere 14 (3). https://doi.org/10.3390/atmos14030488.

Candeo, S., Federici, M., Leonardi, M., Straffelini, G., 2021a. Brake performance maps for a Cu-free friction material with different scorching conditions. Tribol. Trans. 64 (3) https://doi.org/10.1080/10402004.2020.1869360.

Candeo, S., Nogueira, A.P., Leonardi, M., Straffelini, G., 2021b. A study of friction, wear and particulate emissions during the bedding stage of a Cu-free friction material. Wear 486, 487. https://doi.org/10.1016/j.wear.2021.204095.

Chen, K., Yu, L., 2007. Microscopic traffic-emission simulation and case study for evaluation of traffic control strategies. Journal of Transportation Systems Engineering and Information Technology 7 (1). https://doi.org/10.1016/S1570-6672(07)60011-7.

Chen, Y., Wen, C., Jiang, C., Jiang, X., 2021. Global sensitivity analysis of VISSIM parameters for project-level traffic emissions: a case study at a signalized intersection. Environ. Technol. https://doi.org/10.1080/09593330.2021.1934737.

De Kok, T.M., Hogervorst, J.G., Briedé, J.J., Van Herwijnen, M.H., Maas, L.M., Moonen, E.J., Driece, H.A., Kleinjans, J.C., 2005. Genotoxicity and physicochemical characteristics of traffic-related ambient particulate matter. Environ. Mol. Mutagen. 46 (2) https://doi.org/10.1002/em.20133.

EC, 2013. A Clean Air Programme for Europe. Communication from the Commission to the European Parliament, the Council, the European Economic and Social Committee and the Committee of the Regions. COM (2013) 918 Final. EC Brussels, Belgium.

EC, 2023. European Vehicle Emissions Standards – Euro 7 for Cars, Vans, Lorries and Buses. European Commission. https://ec.europa.eu/info/law/better-regulation/have-your-say/initiatives/12313-European-vehicle-emissions-standards-Euro-7-for-cars-vans-lorries-and-buses_en.

Grigoratos, T., Giorgio, M., 2014. Non-exhaust traffic related emissions. Brake and tyre wear PM. In: Non-exhaust Traffic Related Emissions. Brake and tyre wear PM. https://doi.org/10.2790/21481.

Grigoratos, T., Martini, G., 2015. Brake wear particle emissions: a review. Environ. Sci. Pollut. Control Ser. 22 (Issue 4), 2491–2504. https://doi.org/10.1007/s11356-014-3696-8.

Gu, C., Farzaneh, R., Pesti, G., Valdez, G., Birt, A., 2018. Estimating vehicular emission impact of nighttime construction with VISSIM and different MOVES emission estimation approaches. Transport. Res. Rec. 2672 (25) https://doi.org/10.1177/0361198118798988.

Gustafsson, M., Blomqvist, G., Gudmundsson, A., Dahl, A., Swietlicki, E., Bohgard, M., Lindbom, J., Ljungman, A., 2008. Properties and toxicological effects of particles from the interaction between tyres, road pavement and winter traction material. Sci. Total Environ. 393 (2–3) https://doi.org/10.1016/j.scitotenv.2007.12.030.

Han, M.J., Lee, C.H., Park, T.W., Park, J.M., Son, S.M., 2017. Coupled thermo-mechanical analysis and shape optimization for reducing uneven wear of brake pads. Int. J. Automot. Technol. https://doi.org/10.1007/s12239-017-0100-y.

Hassan, A.K.F., Mohammed, S., 2016. Artificial neural network model for estimation of wear and temperature in pin-disc contact. Universal Journal of Mechanical Engineering. https://doi.org/10.13189/ujme.2016.040204.

Hausberger, S., Rexeis, M., Zallinger, M., Luz, R., 2009. Emission Factors from the Model PHEM for the HBEFA Version 3, vol. I. Graz University of Technology.

Hirschmann, K., Zallinger, M., Fellendorf, M., Hausberger, S., 2010. A new method to calculate emissions with simulated traffic conditions. IEEE Conference on Intelligent Transportation Systems, Proceedings, ITSC. https://doi.org/10.1109/ITSC.2010.5625030.

Hula, A., Maguire, A., Bunker, A., Rojeck, T., Harrison, S., 2021. The 2021 EPA Automotive Trends Report: Greenhouse Gas Emissions, Fuel Economy, and Technology since 1975.

Jie, L., van Zuylen, H., Chen, Y., Viti, F., Wilmink, I., 2013. Calibration of a microscopic simulation model for emission calculation. Transport. Res. C Emerg. Technol. 31 https://doi.org/10.1016/j.trc.2012.04.008.

Karabag, H.H., Ulak, B., Mjogolo, F.J., Kidando, E., Ozguven, E.E., Sando, T., Moses, R., 2020. Estimating the impact of green light optimized speed advisory (Glosa) on exhaust emissions through the integration ofvissim and moves. Adv. Transport. Stud. 52 https://doi.org/10.4399/97888255370311.

Ketzel, M., Omstedt, G., Johansson, C., Düring, I., Gidhagen, L., Lohmeyer, A., Berkowicz, R., Wåhlin, P., 2005. Estimation and Validation of PM2. 5/PM10 Exhaust and Nonexhaust Emission Factors for Street Pollution Modelling. Presentation at the 5th Interntl. Conf. on Urban Air Quality (UAQ 2005), Valencia, Spain, pp. 29–31.

Kraschl-Hirschmann, K., Zallinger, M., Luz, R., Fellendorf, M., Hausberger, S., 2011. A method for emission estimation for microscopic traffic flow simulation. FISTS 2011. In: 2011 IEEE Forum on Integrated and Sustainable Transportation Systems. https://doi.org/10.1109/FISTS.2011.5973625.

Kuklinska, K., Wolska, L., Namiesnik, J., 2015. Air quality policy in the U.S. and the EU - a review. Atmos. Pollut. Res. 6 (1) https://doi.org/10.5094/APR.2015.015.

Kutlimuratov, K., Khakimov, S., Mukhitdinov, A., Samatov, R., 2021. Modelling traffic flow emissions at signalized intersection with PTV vissim. E3S Web of Conferences 264. https://doi.org/10.1051/e3sconf/202126402051.

Mantecca, P., Farina, F., Moschini, E., Gallinotti, D., Gualtieri, M., Rohr, A., Sancini, G., Palestini, P., Camatini, M., 2010. Comparative acute lung inflammation induced by atmospheric PM and size-fractionated tire particles. Toxicol. Lett. 198 (2) https://doi.org/10.1016/j.toxlet.2010.07.002.

Mathissen, M., Grigoratos, T., Lahde, T., Vogt, R., 2019. Brake Wear Particle Emissions of a Passenger Car Measured on a Chassis Dynamometer. *Atmosphere*. https://doi.org/10.3390/atmos10090556.

Mathissen, M., Grochowicz, J., Schmidt, C., Vogt, R., Farwick zum Hagen, F.H., Grabiec, T., Steven, H., Grigoratos, T., 2018. A novel real-world braking cycle for studying brake wear particle emissions. Wear. https://doi.org/10.1016/j.wear.2018.07.020.

Men, Z., Zhang, X., Peng, J., Zhang, J., Fang, T., Guo, Q., Wei, N., Zhang, Q., Wang, T., Wu, L., Mao, H., 2022. Determining factors and parameterization of brake wear particle emission. J. Hazard Mater. 434 https://doi.org/10.1016/j.jhazmat.2022.128856.

Moradi, E., 2021. A Machine Learning Methodology for Developing Microscopic Vehicular Fuel Consumption and Emission Models for Local Conditions Using Real-World Measures. McGill University, Canada.

Moradi, E., Miranda-Moreno, L., 2020. Vehicular Fuel Consumption Estimation Using Real-World Measures through Cascaded Machine Learning Modeling, vol. 88. Transportation Research Part D: Transport and Environment. https://doi.org/10.1016/j.trd.2020.102576.

Mukherjee, A., Agrawal, M., 2017. World air particulate matter: sources, distribution and health effects. Environ. Chem. Lett. 15 (Issue 2) https://doi.org/10.1007/s10311-017-0611-9.

Noland, R.B., Quddus, M.A., 2006. Flow improvements and vehicle emissions: effects of trip generation and emission control technology. Transport. Res. Transport Environ. 11 (1) https://doi.org/10.1016/j.trd.2005.06.003.

Pariota, L., Coppola, A., di Costanzo, L., di Vico, A., Andolfi, A., D'Aniello, C., Bifulco, G. N., 2020. Integrating tools for an effective testing of connected and automated vehicles technologies. IET Intell. Transp. Syst. 14 (9) https://doi.org/10.1049/iet-its.2019.0678.

PTV Group, 2022. PTV Vissim 2022 User Manual. Ptv Ag.

Rahimi, M., 2023. Modeling and Simulation of Vehicle Emissions for the Reduction of Road Traffic Pollution [Ph.D. Dissertation]. University of Trento.

Rahimi, M., Bortoluzzi, D., Biral, F., 2022. Impacts of Vehicle Speed and Number of Heavy Vehicles on Emissions and Fuel Consumption in Sensitive Locations. Transportation Research Record, 03611981221137586. https://doi.org/10.1177/03611981221137586.

Rahimi, M., Bortoluzzi, D., Wahlström, J., 2021. Input parameters for airborne brake wear emission simulations: a comprehensive review. Atmosphere 12 (7). https://doi.org/10.3390/atmos12070871.

Rajamani, R., 2011. Vehicle Dynamics and Control. Springer Science & Business Media.

Riva, G., Valota, G., Perricone, G., Wahlström, J., 2019. An FEA approach to simulate disc brake wear and airborne particle emissions. Tribol. Int. 138, 90–98. https://doi.org/10.1016/j.triboint.2019.05.035.

Sabbir Ahmed, C.M., Jiang, H., Chen, J.Y., Lin, Y.H., 2018. Traffic-related particulate matter and cardiometabolic syndrome: a review. Atmosphere 9 (Issue 9). https://doi.org/10.3390/atmos9090336.

Salamati, K., Rouphail, N.M., Frey, H.C., Liu, B., Schroeder, B.J., 2015. Simplified method for comparing emissions in roundabouts and at signalized intersections. Transport. Res. Rec. 2517 https://doi.org/10.3141/2517-06.

Sanders, P.G., Dalka, T.M., Basch, R.H., 2001. A reduced-scale brake dynamometer for friction characterization. Tribol. Int. https://doi.org/10.1016/S0301-679X(01)00053-6.

Sanders, P.G., Dalka, T.M., Xu, N., Maricq, M.M., Basch, R.H., 2002. Brake dynamometer measurement of airborne brake wear debris. In: SAE Technical Papers. https://doi.org/10.4271/2002-01-1280.

Singh, V., Biswal, A., Kesarkar, A.P., Mor, S., Ravindra, K., 2020. High resolution vehicular PM10 emissions over megacity Delhi: relative contributions of exhaust and non-exhaust sources. Sci. Total Environ. 699 https://doi.org/10.1016/j.scitotenv.2019.134273.

So, J. (Jason), Motamedidehkordi, N., Wu, Y., Busch, F., Choi, K., 2018. Estimating emissions based on the integration of microscopic traffic simulation and vehicle dynamics model. International Journal of Sustainable Transportation 12 (4). https://doi.org/10.1080/15568318.2017.1363328.

Song, Z., Wang, H., Sun, J., Tian, Y., 2020. Experimental findings with VISSIM and TransModeler for evaluating environmental and safety impacts using micro-simulations. Transport. Res. Rec. 2674 (8) https://doi.org/10.1177/0361198120925077.

Stevanovic, A., Stevanovic, J., Zhang, K., Batterman, S., 2009. Optimizing Traffic Control to Reduce Fuel Consumption and Vehicular Emissions: Integrated Approach with VISSIM, CMEM, and VISGAOST, vol. 2128. Transportation Research Record. https://doi.org/10.3141/2128-11.

Timmers, V.R.J.H., Achten, P.A.J., 2016. Non-exhaust PM emissions from electric vehicles. Atmos. Environ. 134, 10–17. https://doi.org/10.1016/j.atmosenv.2016.03.017.

Tuan Hoang, A., Nižetić, S., Chyuan Ong, H., Tarelko, W., Viet Pham, V., Hieu Le, T., Quang Chau, M., Phuong Nguyen, X., 2021. A review on application of artificial neural network (ANN) for performance and emission characteristics of diesel engine fueled with biodiesel-based fuels. Sustain. Energy Technol. Assessments 47. https://doi.org/10.1016/j.seta.2021.101416.

UNECE, 2022. Proposal for a New UN GTR on Laboratory Measurement of Brake Emissions for Light-Duty Vehicles. United Nations Economic Commission for Europe. https://unece.org/transport/documents/2022/10/working-documents/iwg-pmp-proposal-new-un-gtr-laboratory-measurement.

Varriale, F., Candeo, S., Riva, G., Wahlström, J., Lyu, Y., 2022. A brake system coefficient of friction estimation using 3D friction maps. Lubricants 10 (7), 134.

Vasiljević, S., Glišović, J., Stojanović, N., Grujić, I., 2022. Application of neural networks in predictions of brake wear particulate matter emission. Proc. Inst. Mech. Eng. - Part D J. Automob. Eng. 236 (7) https://doi.org/10.1177/09544070211036321.

Wahlström, J., Söderberg, A., Olofsson, U., 2009. Simulation of Airborne Wear Particles from Disc Brakes. SAE Technical Paper.

Wang, L., Zhong, B., Vardoulakis, S., Zhang, F., Pilot, E., Li, Y., Yang, L., Wang, W., Krafft, T., 2016. Air quality strategies on public health and health equity in Europe—a systematic review. Int. J. Environ. Res. Publ. Health 13 (Issue 12). https://doi.org/10.3390/ijerph13121196.

Ziemska, M., 2021. Exhaust emissions and fuel consumption analysis on the example of an increasing number of hgvs in the port city. Sustainability 13 (13). https://doi.org/10.3390/su13137428.